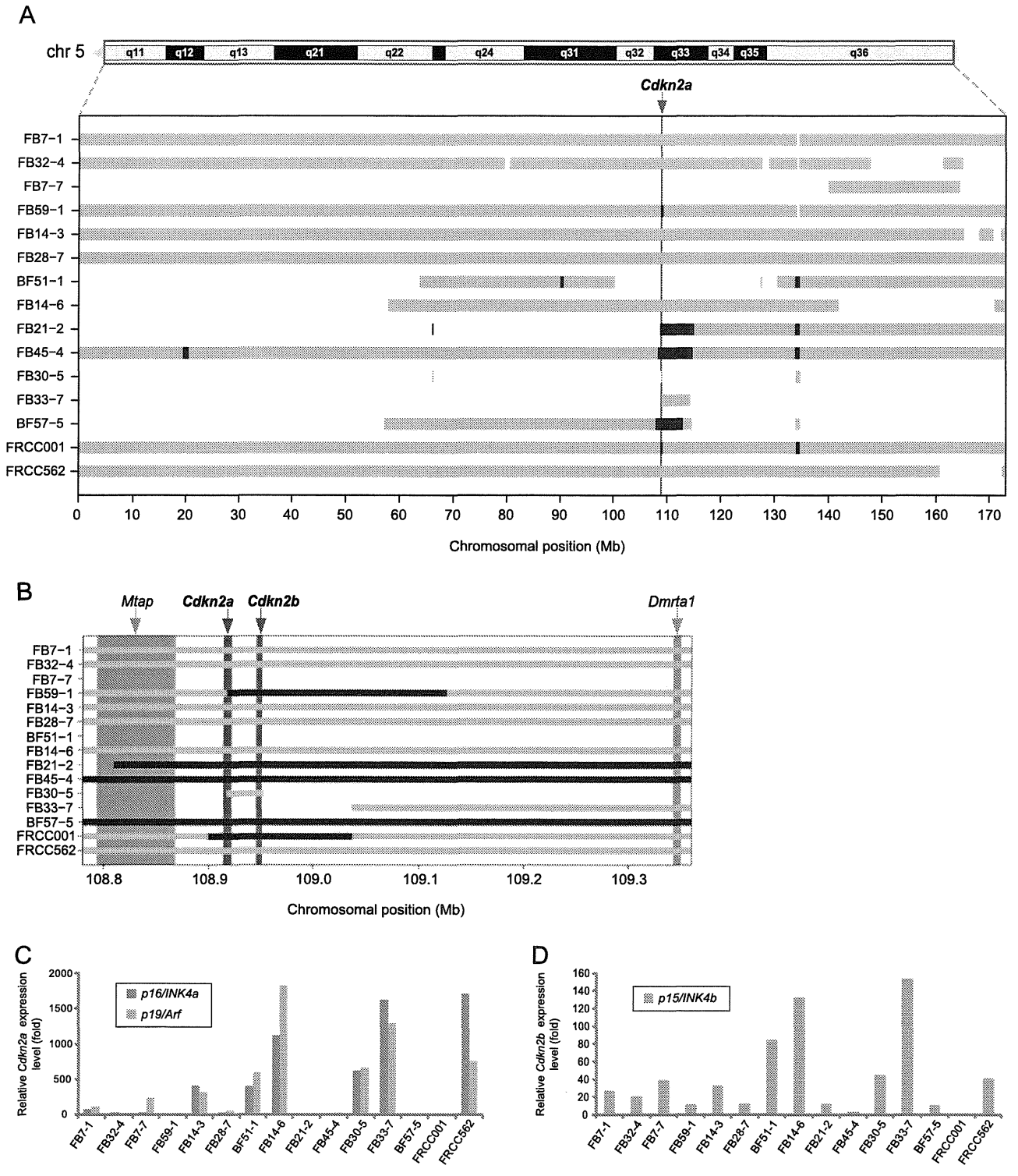

Figure 2. Frequent extensive chromosomal losses in rat chromosome 5, and homozygous deletions at the region including the *Cdkn2a* and *Cdkn2b* loci. (A) The bar chart represents the regions of chromosomal loss (green yellow) and homozygous deletion (dark green) along chromosome 5 for 13 RCC tumors and two RCC cell lines. The vertical red line on the background indicates the position of the *Cdkn2a* locus. (B) Magnified view of the bar chart centered on the *Cdkn2a/2b* loci. The genomic regions of all of the RefSeq genes included in the displayed range of the chromosome are depicted as vertical bars on the background. (C) Expression analysis of *Cdkn2a* ($p16^{Ink4a}$ and $p19^{Arf}$) for 13 RCC tumors and two RCC cell lines, using real-time PCR with specific primer pairs for each different transcript. The values on the *y*-axis indicate relative mRNA expression level compared to an average of those in normal kidneys of three control rats. (D) Expression analysis of *Cdkn2b* ($p15^{Ink4b}$) for 13 RCC tumors and two RCC cell lines by real-time PCR. The values on the *y*-axis indicate relative mRNA expression level compared to an average of those in normal kidneys of three control rats.

doi:10.1371/journal.pone.0043403.g002

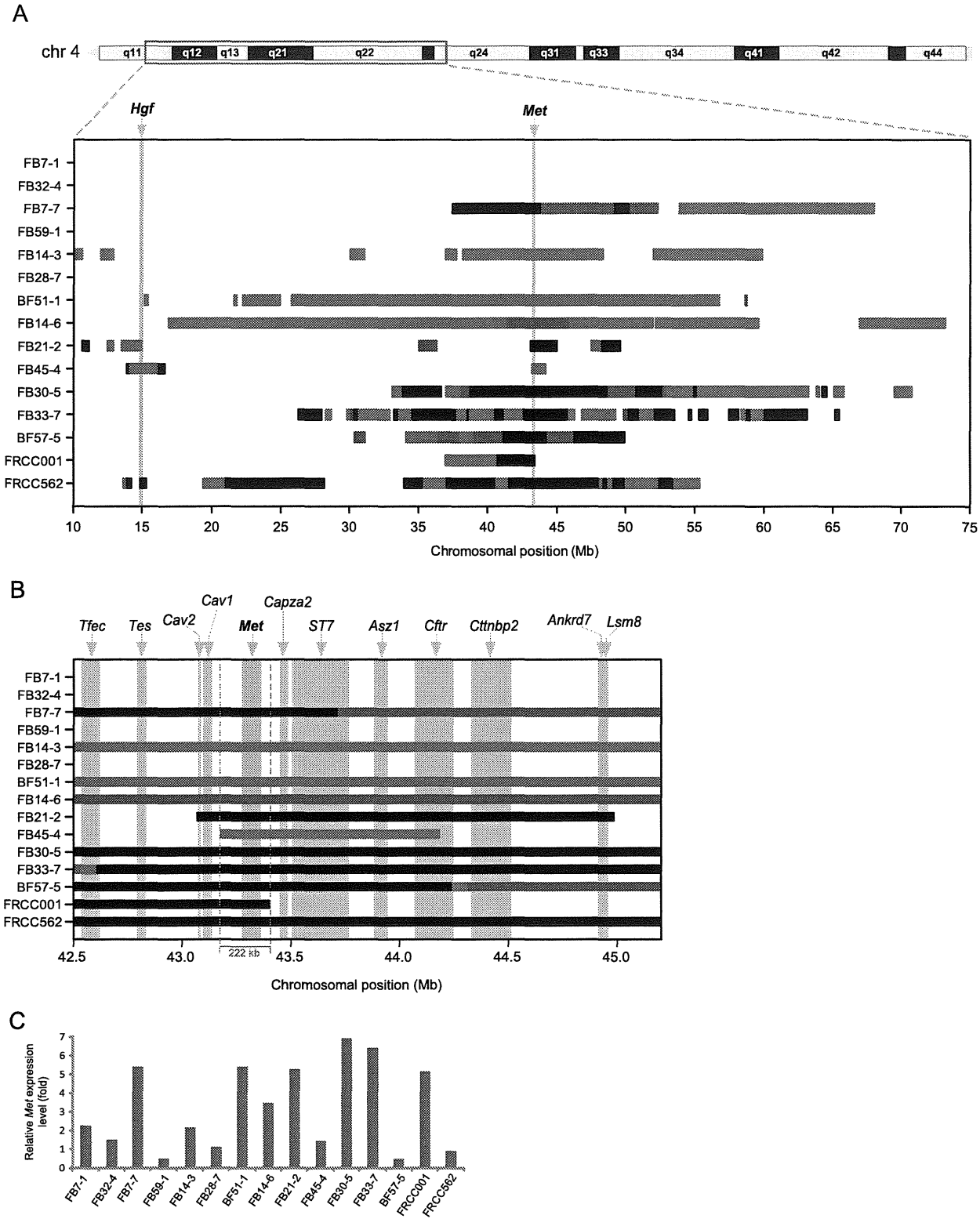

Figure 3. Frequent wide-ranging amplifications over a long pericentromeric region of chromosome 4 with the *Met* oncogene residing in the most overlapping section. (A) The bar chart represents the amplification regions along a 65 Mb pericentrometic region of chromosome 4 for 13 RCC tumors and two RCC cell lines. Four grades of amplification are indicated by bar color gradation; the darker the red, the larger the amplitude. (B) A magnified view of the bar chart above shows the vicinity of the most overlapping region. The genomic regions of all of the RefSeq genes included in the displayed range of the chromosome are depicted as vertical bars in the background. (C) Expression analysis of *Met* for 13 RCC tumors and two RCC cell lines by real-time PCR. The values on the *y*-axis indicate relative mRNA expression level compared to an average of those in normal kidneys of three control rats.
doi:10.1371/journal.pone.0043403.g003

Table 1. Features of 13 cases of Fe-NTA-induced renal cell carcinomas.

						Copy number aberration at	
Tumor case	**Size (mm)**	**Metastasis**	**Invasion**	**Nuclear atypia grade**	**Growth pattern**	***Met* locus**	***Cdkn2a/2b* locus**
FB7-1	20	None	None	Low	Intermediate	None	Loss
FB32-4	15	Lung	None	Intermediate	Intermediate	None	Loss
FB7-7	60	Lung	None	Intermediate	Expansive	Amplification	None
FB59-1	15	Lung	Peritoneal	Intermediate	Infiltrating	None	HD
FB14-3	15	None	None	High	Expansive	Amplification	Loss
FB28-7	30	None	None	High	Intermediate	None	Loss
BF51-1	28	None	None	High	Intermediate	Amplification	None
FB14-6	30	Lung	Peritoneal	High	Intermediate	Amplification	Loss
FB21-2	40	None	None	High	Infiltrating	Amplification	HD
FB45-4	40	Lung	None	High	Infiltrating	Amplification	HD
FB30-5	60	Lung	Peritoneal	High	Infiltrating	Amplification	Loss
FB33-7	70	Lung	Peritoneal	High	Infiltrating	Amplification	None
BF57-5	25	Lung	Peritoneal	High	Infiltrating	Amplification	HD

Fe-NTA: ferric nitrilotriacetate; HD: homozygous deletion.
doi:10.1371/journal.pone.0043403.t001

or subtle genetic alterations (**Fig. S5**). Accordingly, oxidative stress, including that induced due to excess iron, could be one of the causes of human renal carcinogenesis. Indeed, numerous epidemiological studies have associated iron and steel industry workers with an increased RCC risk [35].

A frequency plot analysis revealed two remarkable features. First, the chromosomal aberrations showed a preference for loss against the ploidy of each cancer genome. Mostly, the aberration was represented by a deletion at either a whole chromosomal level (monosomy) or at a segmental level (**Fig. 1B**). The most common target for loss was the *Cdkn2a/2b* locus. The predominance of loss in the profile of chromosomal alterations may be attributed to the early stage of carcinogenesis. We previously demonstrated that cells with a hemizygous deletion at *Cdkn2a* appear as early as a few weeks after initiating a Fe-NTA administration [36].

Our present analysis revealed that the monoallelic loss of chromosome 5 in its entirety or of an equivalently wide region is the major first event. Indeed, we found only one case (6.7%) of a monoallelic loss of an extremely narrow region (~350 kilobases; **Figs. 2A and 2B**). Fe-NTA catalyzes the generation of hydroxyl radicals through a Fenton reaction specifically in the lumina of renal proximal tubules, which leads to degeneration and necrosis/apoptosis of those cells [37,38]. Because kidney is a vital organ that performs urea excretion, reabsorption of valuable molecules as

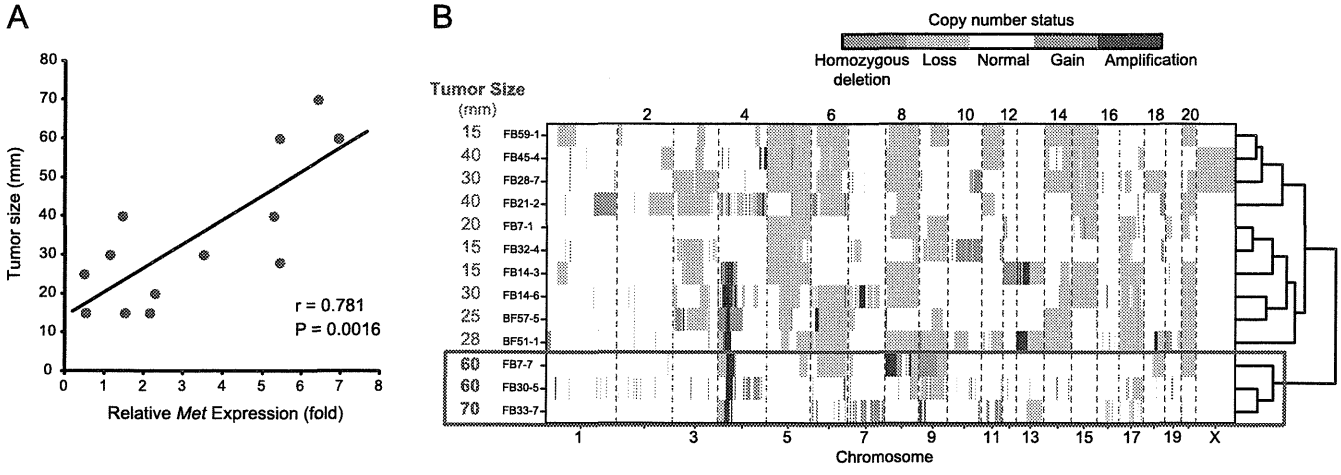

Figure 4. Tumor sizes of Fe-NTA induced RCCs are controlled by the genetic features. (A) *Met* expression is significantly correlated with tumor size. Pearson's correlation coefficient (r) and the corresponding P value are written on the plot area. (B) Hierarchical clustering of the RCC tumors based on the whole genome patterns of the copy number changes. The large-size tumors form a distinct cluster.
doi:10.1371/journal.pone.0043403.g004

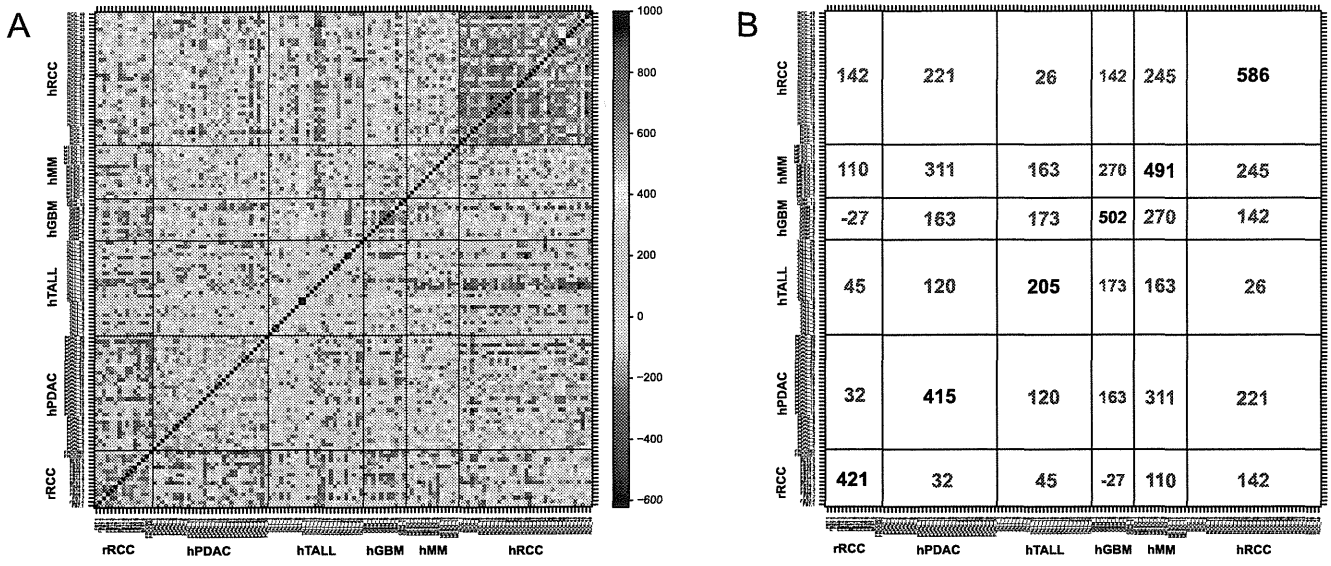

Figure 5. Comparison of copy number alteration profiles in cancer genomes between Fe-NTA-induced rat RCCs and human tumors. (A) The color plot represents a similarity matrix across the rat RCCs and various human cancers. rRCC, rat renal cell carcinoma; hPDAC, human pancreatic ductal adenocarcinoma; hTALL, human T-cell acute lymphoblastic leukemia; hGBM, human glioblastoma multiforme; hRCC, human renal cell carcinoma. (B) Numerical summary of the similarity matrix. The number in each square indicates an average value of similarity index (defined between −1000 and 1,000). Refer to the Materials and Methods section for details.
doi:10.1371/journal.pone.0043403.g005

well as ionic homeostasis maintenance, regeneration from the remaining tubular cells is intensely promoted. Under chronic oxidative stress by repeated Fe-NTA administrations, this degeneration and regeneration process would continue for months to years, increasing the risk of mitotic events simultaneously with the repair of oxidative DNA damage. We believe that this oxidative stress causes abnormal DNA replication and chromosomal missegregation, which leads to the emergence of aneuploid cells. Surprisingly, this series of events appear to occur in months, leading to a high incidence (~90%) of RCC in rats within two years. Aneuploid cells usually exhibit phenotypes consistent with increased energy need and proteotoxic stress. However, aneuploidy can promote tumorigenesis under the following two hypothetical mechanisms: 1) aneuploidy may cause a proliferative advantage through loss of G1/S transition control under conditions in which normal euploid cells do not divide [39] and 2) aneuploidy can advance tumorigenesis by promoting genomic instability, hence increasing the evolvability of tumors [40]. The frequent deletion of the *Cdkn2a/2b* locus is observed in the rat peritoneal mesothelioma, an iron overload-associated tumor [41], induced either by another iron compound (ferric saccharate) [42] or by asbestos [43]. These common traits of animal models strongly suggest that *Cdkn2a/2b* is a principal target in iron-mediated carcinogenesis. The same genetic alteration is observed in rat mesothelioma induced by multi-walled carbon nanotubes [44], in which iron involvement is not yet established. We would like to add here for the biological significance of our results that homozygous deletion of *CDKN2A/2B* is frequently observed in human mesothelioma associated with asbestos exposure [**45,46**].

Some of the tumors with a remaining *Cdkn2a/2b* allele showed extremely high expression levels of two products from this locus, *p16/Ink4a* and *p19/Arf*. This is a currently debated issue in human cancer [47]. There is considerable evidence that several neoplasms exhibit significant p16 levels in cytoplasm [48]. This can be an unsuccessful attempt to stop cell proliferation in the case of downstream *Rb* dysregulation [49] or may represent an alternative mechanism for modulating unidentified pathways. Our data exhibit ~50% hemizygous deletion of *Rb*. This requires further clarification with epigenetic analysis.

The second feature determined using frequency plot analysis was a high incidence of amplification along a limited chromosomal region toward the centromere of chromosome 4, pointing to the *Met* locus. A region spanning 80 Mb from the centromere of rat chromosome 4 is syntenic to human chromosome 7. Various human cancers, such as glioblastoma [50] and non-small cell lung cancer [51], are reported to harbor amplifications in chromosome 7. Tyrosine kinase MET is a receptor for a hepatocyte growth factor and is situated upstream of *ras* in the signal transduction pathway, thus serving as an advantage for cell proliferation [52]. Therefore, it is conceivable that tumor size was proportionally associated with the *Met* expression level (**Figs. 3C and 4A**). Because we dissect the animal as soon as we recognize the tumor, we believe that large-sized tumors are more aggressive in nature. It is of note that tumor size was also related to the genome alteration pattern (**Fig. 4B**), and was associated with amplification and overexpression of *Zbtb38* located on chromosome 8 (**Fig. S4**). ZBTB38 (CIBZ) represses the transcription of methylated templates [53], thus presumably regulating epigenetic mechanisms. Down-regulation of ZBTB38, a novel substrate of caspase-3, induces apoptosis [54] and this gene is localized in a prostate cancer susceptibility locus [54]. These results confirm the possibility of tumor classification using array-based CGH. *Met* arose evolutionally late and is unique to mammals [52]; it could thereby be associated with the unique amplification in the whole genome.

Genomic amplification is hypothesized to occur via the breakage-fusion-bridge cycle [55,56,57]. A Fenton reaction causes double-stranded DNA breakage [10]. Our results revealed that these amplifications consisted of a mixture of wide-range low-level amplifications and fragmented, narrow high-level amplifications

(**Fig. 3A**). This suggests a mechanism of positive feedback for amplification, starting from wide-range low-level amplification. We suspect an involvement of double-minutes, and a presence of susceptible genomic loci. This hypothesis requires further study. It was interesting that two tumor suppressive genes, *Cav1* [58,59] and *ST7* [60], surrounded the *Met* locus (**Fig. 3B**). This may be the reason why the *Met* locus was a denominator for the rat RCCs. Whole exome or genome sequencing may further reveal new findings regarding point mutation and chromosomal translocation.

Finally, we compared the present rat results with corresponding human tumors by transforming data based on chromosomal synteny (**Figs. 5A and 5B**). It was expected that the genomic alteration of Fe-NTA-induced rat RCC was most similar to human RCC presumably because target cells are the same. However, surprisingly, human mesothelioma was the second most similar. It is now established that most human mesothelioma results from exposure to asbestos, and the primary pathogenic process involved is iron overload [**8,61**]. The same mesodermal origin of renal tubular cells and mesothelial cells may cause the similarity of the array-based CGH profiles. Endodermal tumor, such as pancreatic ductal adenocarcinoma (PDAC), and ectodermal tumor, such as glioblastoma multiforme (GBM), exhibited a significant difference in genomic profiles.

In conclusion, we showed that repeated Fenton reactions in wild-type rats induced cancer that recapitulated genomic alterations similar to those in human cancers, suggesting the involvement of oxidative stress as a major factor in human carcinogenesis. In this renal carcinogenesis model, preferred alterations were deletion; *Cdkn2A/2B* deletion and *Met* amplification were the major target gene modifications. A comparative interspecies analysis would contribute to identifying candidate carcinogenic agents.

Materials and Methods

Fe-NTA-induced Renal Cell Carcinoma Model

Fe-NTA-induced carcinogenesis experiments were performed using male F1 hybrid rats that were a cross between Fischer 344 and Brown-Norway inbred strains (Charles River, Yokohama, Japan) as previously described [62]. Thirteen RCC cases were used in this study, and the histological grade of the tumor was determined according to the modified World Health Organization classification as we previously described [62]. The details are summarized in **Table 1**. The animal experiment committees of the Graduate School of Medicine, Kyoto University Graduate School of Medicine and Nagoya University Graduate School of Medicine approved this study. FRCC001 and FRCC562 cell lines were established from primary Fe-NTA-induced RCCs as previously described [63].

Array-based Comparative Genomic Hybridization

Genomic DNA from the tumors and the cell lines was isolated with DNeasy (Qiagen, Valencia, CA). Array-based CGH was performed with an Agilent 185 K rat genome CGH microarray (Agilent Technologies, Santa Clara, CA) as previously described [64]. Thirteen primary tumors and two cell lines of Fe-NTA induced RCCs were analyzed using reference DNA extracted from a normal kidney of a rat from Brown-Norway imbred strain. One RCC sample of a female Eker rat [32] was analyzed using reference DNA extracted from a normal kidney of a male Eker rat. Two additional RCC samples of male Eker rats were analyzed with Rat Genome CGH Microarray 105A (G4436A; Agilent Technologies), using reference DNA extracted from a normal liver of another male Eker rat. The normalized array-based CGH data were processed to generate a segmented profile by circular binary segmentation (CBS) [65] with an altered significance level (alpha = 0.0001). The procedure of data processing for copy number estimation is detailed in **Methods S1**.

Quantitative RT-PCR Analysis

Total RNA was isolated using Isogen reagents (Nippon Gene Co. Ltd., Tokyo, Japan) according to the manufacturer's protocol. cDNA was synthesized using an RNA PCR kit ver. 3.0 (Takara Bio, Shiga, Japan) with random primers. A Platinum SYBR Green qPCR SuperMix-UDG kit (Invitrogen, Carlsbad, CA) and a 7300 Real-Time PCR System (Applied Biosystems, Foster City, CA) were used for quantitative real-time PCR analysis. Rat β-actin was used as an internal control. The primers used were as follows: $p16^{Ink4a}$, 5′-aaacgccccgaacactttc-3′ and 5′-gttcgaatctgcaccatagga-3′; $p19^{Arf}$, 5′-accccaagtgagggttttct-3′ and 5′-agagctgccactttgacgtt-3′; $p15^{Ink4b}$, 5′-tccacaggctagagggaaaa-3′ and 5′-gtgcaggtgactccttggtt-3′; *Met*, 5′-ttaagcgagagcacgacaaat-3′ and 5′-ccacataggaaaacgcactgt-3′; *Zbtb38*, 5′-gtagctgctgctccaaatcc-3′ and 5′-cctgttgagggtggtgaact-3′; β-actin, 5′-tgtgttgtccctgtatgcctctg-3′ and 5′-atagatgggcacagtgtgggtg-3′.

Human Data

We used human array-based CGH data of pancreatic ductal adenocarcinoma (hPDAC) [28], T-cell acute lymphoblastic leukemia (hTALL) [28], glioblastoma (hGBM) [66], mesothelioma cell line (hMM) [67] and renal cell carcinoma (hRCC) [56]. The Agilent CGH-array data of the former four types of human cancer were obtained from NCBI's Gene Expression Omnibus (GEO) website (http://www.ncbi.nlm.nih.gov/geo/). The GEO accession numbers for the data sets are GSE7599 (hPDAC), GSE7603 (hTALL), GSE9177 (hGBM) and GSE22237 (hMM). The human RCC data was obtained through analyses with BAC microarrays (4,361 clones) [68]. We defined similarity index between the two array-based CGH profiles as follows. First, we calculated the correlation coefficient with log2 ratios of the estimated copy number over the inferred cancer ploidy for the genomic positions corresponding to all of the Agilent 44 K human CGH microarray probes. Then, we multiplied the value by 1×10^3 after changing the absolute value into its square root.

Supporting Information

Figure S1 Array-CGH profiles from all the RCCs examined. Red lines show log2 ratios of estimated copy number over inferred cancer ploidy versus genomic position for all the CGH microarray probes.
(PDF)

Figure S2 Distribution of log2 ratio values of estimated copy number for all the probes in all the microarrays performed.
(PDF)

Figure S3 Example of global expression changes in line with genomic alteration. Differences in genome and transcriptome are analyzed between two RCCs, FB7-7 having wide-range amplification on chromosome 4 versus FB28-7 having no substantial genomic alteration on chromosome 4. (A) Sky blue circle plot indicates ratio of estimated copy numbers based on array-based CGH (FB7-7 *vs* FB28-7). Red circle plot indicates ratio of normalized signals on Affymetrix expression microarray (FB7-7 *vs* FB28-7). (B) Expression ratio values are averaged along the chromosome. Here, red circle plot indicates average value in 2-Mb windows.
(PDF)

Figure S4 *Zbtb38* mRNA expression is demonstrably associated with its chromosomal copy number. (A) Array-CGH profiles of two RCC tumors harboring amplification over *Zbtb38* locus on chromosome 8. (B) Expression analysis of *Zbtb38* on 13 RCC tumors by real-time PCR. The values of the *y*-axis indicate the relative mRNA expression level compared to an average of those in normal kidneys of three control rats.
(PDF)

Figure S5 Array-CGH profiles of three hereditary (Eker rat) renal tumors. Red lines show log2 ratios of estimated copy number over inferred cancer ploidy versus genomic position for all the CGH microarray probes.
(PDF)

Table S1 List of genes completely deleted in more than two RCC tumors.
(XLS)

Table S2 List of genes amplified in more than two RCC tumors.
(XLS)

Methods S1 Supplementary methods.
(DOC)

Author Contributions

Conceived and designed the experiments: SA ST. Performed the experiments: SA YY HO YTL MI KA MO LJ H. Nagai HM EA. Analyzed the data: SA YO TT ST. Contributed reagents/materials/analysis tools: YS YK OH H. Nakagama. Wrote the paper: SA ST. Designed the software used in analysis: SA.

References

1. Weinberg RA (2007) The biology of cancer. New York: Garland Science, Tailor & Francis Group, LLC.
2. Klijn C, Holstege H, de Ridder J, Liu X, Reinders M, et al. (2008) Identification of cancer genes using a statistical framework for multiexperiment analysis of nondiscretized array CGH data. Nucleic Acids Res 36: e13.
3. Parsons DW, Jones S, Zhang X, Lin JC, Leary RJ, et al. (2008) An integrated genomic analysis of human glioblastoma multiforme. Science 321: 1807–1812.
4. Pfeifer GP, Hainaut P (2011) Next-generation sequencing: emerging lessons on the origins of human cancer. Curr Opin Oncol 23: 62–68.
5. Toyokuni S (1999) Reactive oxygen species-induced molecular damage and its applicaton in pathology. PatholInt 49: 91–102.
6. Halliwell B, Gutteridge JMC (2007) Free radicals in biology and medicine. New York: Oxford University Press.
7. Toyokuni S (1996) Iron-induced carcinogenesis: the role of redox regulation. Free Radic Biol Med 20: 553–566.
8. Toyokuni S (2009) Role of iron in carcinogenesis: Cancer as a ferrotoxic disease. Cancer Sci 100: 9–16.
9. Fenton HJH (1894) Oxidation of tartaric acid in presence of iron. J Chem Soc 65: 899–910.
10. Toyokuni S, Sagripanti JL (1992) Iron-mediated DNA damage: sensitive detection of DNA strand breakage catalyzed by iron. J Inorg Biochem 47: 241–248.
11. Ebina Y, Okada S, Hamazaki S, Ogino F, Li JL, et al. (1986) Nephrotoxicity and renal cell carcinoma after use of iron- and aluminum- nitrilotriacetate complexes in rats. J Natl Cancer Inst 76: 107–113.
12. Li JL, Okada S, Hamazaki S, Ebina Y, Midorikawa O (1987) Subacute nephrotoxicity and induction of renal cell carcinoma in mice treated with ferric nitrilotriacetate. Cancer Res 47: 1867–1869.
13. Toyokuni S, Mori T, Dizdaroglu M (1994) DNA base modifications in renal chromatin of Wistar rats treated with a renal carcinogen, ferric nitrilotriacetate. Int J Cancer 57: 123–128.
14. Toyokuni S, Tanaka T, Hattori Y, Nishiyama Y, Ochi H, et al. (1997) Quantitative immunohistochemical determination of 8-hydroxy-2′-deoxyguanosine by a monoclonal antibody N45.1: its application to ferric nitrilotriacetate-induced renal carcinogenesis model. Lab Invest 76: 365–374.
15. Toyokuni S, Uchida K, Okamoto K, Hattori-Nakakuki Y, Hiai H, et al. (1994) Formation of 4-hydroxy-2-nonenal-modified proteins in the renal proximal tubules of rats treated with a renal carcinogen, ferric nitrilotriacetate. Proc Natl Acad Sci USA 91: 2616–2620.
16. Toyokuni S, Luo XP, Tanaka T, Uchida K, Hiai H, et al. (1997) Induction of a wide range of C_{2-12} aldehydes and C_{7-12} acyloins in the kidney of Wistar rats after treatment with a renal carcinogen, ferric nitrilotriacetate. Free Radic Biol Med 22: 1019–1027.
17. Gutteridge J, Rowley D, Halliwell B (1981) Superoxide-dependent formation of hydroxyl radicals in the presence of iron salts. Detection of 'free' iron in biological systems by using bleomycin-dependent degradation of DNA. Biochem J 199: p263–265.
18. Sasaki K, Ikuta K, Tanaka H, Ohtake T, Torimoto Y, et al. (2011) Improved quantification for non-transferrin-bound iron measurement using high-performance liquid chromatography by reducing iron contamination. Mol Med Report 4: 913–918.
19. Tanaka T, Iwasa Y, Kondo S, Hiai H, Toyokuni S (1999) High incidence of allelic loss on chromosome 5 and inactivation of $p15^{INK4B}$ and $p16^{INK4A}$ tumor suppressor genes in oxystress-induced renal cell carcinoma of rats. Oncogene 18: 3793–3797.
20. Toyokuni S, Akatsuka S (2006) What has been learned from the studies of oxidative stress-induced carcinogenesis: Proposal of the concept of oxygenomics. J Clin Biochem Nutr 39: 3–10.
21. Kallioniemi A, Kallioniemi OP, Sudar D, Rutovitz D, Gray JW, et al. (1992) Comparative genomic hybridization for molecular cytogenetic analysis of solid tumors. Science 258: 818–821.
22. Macconaill LE, Van Hummelen P, Meyerson M, Hahn WC (2011) Clinical implementation of comprehensive strategies to characterize cancer genomes: opportunities and challenges. Cancer Discov 1: 297.
23. Negrini S, Gorgoulis VG, Halazonetis TD (2011) Genomic instability–an evolving hallmark of cancer. Nat Rev Mol Cell Biol 11: 220–228.
24. Adamovic T, McAllister D, Guryev V, Wang X, Andrae JW, et al. (2009) Microalterations of inherently unstable genomic regions in rat mammary carcinomas as revealed by long oligonucleotide array-based comparative genomic hybridization. Cancer Res 69: 5159–5167.
25. Femia AP, Luceri C, Toti S, Giannini A, Dolara P, et al. (2010) Gene expression profile and genomic alterations in colonic tumours induced by 1,2-dimethylhydrazine (DMH) in rats. BMC Cancer 10: 194.
26. Takabatake T, Fujikawa K, Tanaka S, Hirouchi T, Nakamura M, et al. (2006) Array-CGH analyses of murine malignant lymphomas: genomic clues to understanding the effects of chronic exposure to low-dose-rate gamma rays on lymphomagenesis. Radiat Res 166: 61–72.
27. Herzog CR, Desai D, Amin S (2006) Array CGH analysis reveals chromosomal aberrations in mouse lung adenocarcinomas induced by the human lung carcinogen 4-(methylnitrosamino)-1-(3-pyridyl)-1-butanone. Biochem Biophys Res Commun 341: 856–863.
28. Maser R, Choudhury B, Campbell P, Feng B, Wong K, et al. (2007) Chromosomally unstable mouse tumours have genomic alterations similar to diverse human cancers. Nature 447: 966–971.
29. Loeb LA, Bielas JH, Beckman RA (2008) Cancers exhibit a mutator phenotype: clinical implications. Cancer Res 68: 3551–3557.
30. Hisada M, Garber JE, Fung CY, Fraumeni JF, Li FP (1998) Multiple primary cancers in families with Li-Fraumeni syndrome. J Natl Cancer Inst 90: 606–611.
31. Gruis NA, van der Velden PA, Sandkuijl LA, Prins DE, Weaver-Feldhaus J, et al. (1995) Homozygotes for CDKN2 (p16) germline mutation in Dutch familial melanoma kindreds. Nat Genet 10: 351–353.
32. Kobayashi T, Hirayama Y, Kobayashi E, Kubo Y, Hino O (1995) A germline insertion in the tuberous sclerosis (Tsc2) gene give rise to the Eker rat model of dominantly inherited cancer. Nature Genet 9: 70–74.
33. Hino O (2004) Multistep renal carcinogenesis in the Eker (Tsc 2 gene mutant) rat model. Curr Mol Med 4: 807–811.
34. Yeung RS (2004) Lessons from the Eker rat model: from cage to bedside. Curr Mol Med 4: 799–806.
35. Huang X (2003) Iron overload and its association with cancer risk in humans: evidence for iron as a carcinogenic metal. Mutat Res 533: 153–171.
36. Hiroyasu M, Ozeki M, Kohda H, Echizenya M, Tanaka T, et al. (2002) Specific allelic loss of p16 (INK4A) tumor suppressor gene after weeks of iron-mediated oxidative damage during rat renal carcinogenesis. Am J Pathol 160: 419–424.
37. Toyokuni S, Okada S, Hamazaki S, Minamiyama Y, Yamada Y, et al. (1990) Combined histochemical and biochemical analysis of sex hormone dependence of ferric nitrilotriacetate-induced renal lipid peroxidation in ddY mice. Cancer Res 50: 5574–5580.
38. Zhang D, Okada S, Yu Y, Zheng P, Yamaguchi R, et al. (1997) Vitamin E inhibits apoptosis, DNA modification, and cancer incidence induced by iron-mediated peroxidation in Wistar rat kidney. Cancer Res 57: 2410–2414.
39. Torres EM, Williams BR, Tang YC, Amon A (2010) Thoughts on aneuploidy. Cold Spring Harb Symp Quant Biol 75: 445–451.
40. Torres EM, Williams BR, Amon A (2008) Aneuploidy: cells losing their balance. Genetics 179: 737–746.
41. Toyokuni S (2009) Mechanisms of asbestos-induced carcinogenesis. Nagoya J Med Sci 71: 1–10.

42. Hu Q, Akatsuka S, Yamashita Y, Ohara H, Nagai H, et al. (2010) Homozygous deletion of *CDKN2A/2B* is a hallmark of iron-induced high-grade rat mesothelioma. Lab Invest 90: 360–373.
43. Jean D, Thomas E, Manie E, Renier A, de Reynies A, et al. (2011) Syntenic relationships between genomic profiles of fiber-induced murine and human malignant mesothelioma. Am J Pathol 178: 881–894.
44. Nagai H, Okazaki Y, Hwu C, Misawa N, Yamashita Y, et al. (2011) Diameter of multi-walled carbon nanotubes is a critical factor in mesothelial injury and subsequent carcinogenesis. Proc Natl Acad Sci USA.
45. Cheng J, Jhanwar S, Klein W, Bell D, Lee W, et al. (1994) p16 alterations and deletion mapping of 9p21-p22 in malignant mesothelioma. Cancer Res 54: 5547–5551.
46. Xio S, Li D, Vijg J, Sugarbaker D, Corson J, et al. (1995) Codeletion of *p15* and *p16* in primary malignant mesothelioma. Oncogene 11: p511–515.
47. Romagosa C, Simonetti S, Lopez-Vicente L, Mazo A, Lleonart ME, et al. (2011) p16(Ink4a) overexpression in cancer: a tumor suppressor gene associated with senescence and high-grade tumors. Oncogene 30: 2087–2097.
48. Evangelou K, Bramis J, Peros I, Zacharatos P, Dasiou-Plakida D, et al. (2004) Electron microscopy evidence that cytoplasmic localization of the p16(INK4A) "nuclear" cyclin-dependent kinase inhibitor (CKI) in tumor cells is specific and not an artifact. A study in non-small cell lung carcinomas. Biotech Histochem 79: 5–10.
49. Reuschenbach M, Waterboer T, Wallin KL, Einenkel J, Dillner J, et al. (2008) Characterization of humoral immune responses against p16, p53, HPV16 E6 and HPV16 E7 in patients with HPV-associated cancers. Int J Cancer 123: 2626–2631.
50. Wullich B, Sattler HP, Fischer U, Meese E (1994) Two independent amplification events on chromosome 7 in glioma: amplification of the epidermal growth factor receptor gene and amplification of the oncogene MET. Anticancer Res 14: 577–579.
51. Campbell JM, Lockwood WW, Buys TP, Chari R, Coe BP, et al. (2008) Integrative genomic and gene expression analysis of chromosome 7 identified novel oncogene loci in non-small cell lung cancer. Genome 51: 1032–1039.
52. Birchmeier C, Birchmeier W, Gherardi E, Vande Woude GF (2003) Met, metastasis, motility and more. Nat Rev Mol Cell Biol 4: 915–925.
53. Filion GJ, Zhenilo S, Salozhin S, Yamada D, Prokhortchouk E, et al. (2006) A family of human zinc finger proteins that bind methylated DNA and repress transcription. Mol Cell Biol 26: 169–181.
54. Oikawa Y, Matsuda E, Nishii T, Ishida Y, Kawaichi M (2008) Down-regulation of CIBZ, a novel substrate of caspase-3, induces apoptosis. J Biol Chem 283: 14242–14247.
55. Hellman A, Zlotorynski E, Scherer SW, Cheung J, Vincent JB, et al. (2002) A role for common fragile site induction in amplification of human oncogenes. Cancer Cell 1: 89–97.
56. Albertson DG (2006) Gene amplification in cancer. Trends Genet 22: 447–455.
57. Martinez AC, van Wely KH (2010) Are aneuploidy and chromosome breakage caused by a CINgle mechanism? Cell Cycle 9: 2275–2280.
58. Wiechen K, Diatchenko L, Agoulnik A, Scharff KM, Schober H, et al. (2001) Caveolin-1 is down-regulated in human ovarian carcinoma and acts as a candidate tumor suppressor gene. Am J Pathol 159: 1635–1643.
59. Wiechen K, Sers C, Agoulnik A, Arlt K, Dietel M, et al. (2001) Down-regulation of caveolin-1, a candidate tumor suppressor gene, in sarcomas. Am J Pathol 158: 833–839.
60. Pal S, Vishwanath SN, Erdjument-Bromage H, Tempst P, Sif S (2004) Human SWI/SNF-associated PRMT5 methylates histone H3 arginine 8 and negatively regulates expression of ST7 and NM23 tumor suppressor genes. Mol Cell Biol 24: 9630–9645.
61. Nagai H, Ishihara T, Lee WH, Ohara H, Okazaki Y, et al. (2011) Asbestos surface provides a niche for oxidative modification. Cancer Sci 102: 2118–2125.
62. Nishiyama Y, Suwa H, Okamoto K, Fukumoto M, Hiai H, et al. (1995) Low incidence of point mutations in *H-*, *K-* and *N-ras* oncogenes and *p53* tumor suppressor gene in renal cell carcinoma and peritoneal mesothelioma of Wistar rats induced by ferric nitrilotriacetate. Jpn J Cancer Res 86: 1150–1158.
63. Tanaka T, Akatsuka S, Ozeki M, Shirase T, Hiai H, et al. (2004) Redox regulation of annexin 2 and its implications for oxidative stess-induced renal carcinogenesis and metastasis. Oncogene 23: 3980–3989.
64. Liu Y-T, Shang D-G, Akatsuka S, Ohara H, Dutta KK, et al. (2007) Chronic oxidative stress causes amplification and overexpresson of *ptprz1* protein tyrosine phosphatase to activate β-catenin pathway. Am J Pathol 171: 1978–1988.
65. Olshen AB, Venkatraman ES, Lucito R, Wigler M (2004) Circular binary segmentation for the analysis of array-based DNA copy number data. Biostatistics 5: 557–572.
66. Wiedemeyer R, Brennan C, Heffernan TP, Xiao Y, Mahoney J, et al. (2008) Feedback circuit among INK4 tumor suppressors constrains human glioblastoma development. Cancer Cell 13: 355–364.
67. Murakami H, Mizuno T, Taniguchi T, Fujii M, Ishiguro F, et al. (2011) LATS2 is a tumor suppressor gene of malignant mesothelioma. Cancer Res 71: 873–883.
68. Arai E, Ushijima S, Tsuda H, Fujimoto H, Hosoda F, et al. (2008) Genetic clustering of clear cell renal cell carcinoma based on array-comparative genomic hybridization: its association with DNA methylation alteration and patient outcome. Clin Cancer Res 14: 5531–5539.

Journal of Pathology
J Pathol 2012; **228:** 366–377
Published online 2 August 2012 in Wiley Online Library
(wileyonlinelibrary.com) DOI: 10.1002/path.4075

ORIGINAL PAPER

Iron overload signature in chrysotile-induced malignant mesothelioma

Li Jiang,[1] Shinya Akatsuka,[1] Hirotaka Nagai,[1,2] Shan-Hwu Chew,[1] Hiroki Ohara,[1,2] Yasumasa Okazaki,[1] Yoriko Yamashita,[1] Yutaka Yoshikawa,[3] Hiroyuki Yasui,[3] Katsuya Ikuta,[4] Katsunori Sasaki,[5] Yutaka Kohgo,[4] Seishiro Hirano,[6] Yasushi Shinohara,[7] Norihiko Kohyama,[8] Takashi Takahashi[9] and Shinya Toyokuni[1]*

[1] *Department of Pathology and Biological Responses, Nagoya University Graduate School of Medicine, 65 Tsurumai-cho, Showa-ku, Nagoya 466-8550, Japan*
[2] *Department of Pathology and Biology of Diseases, Graduate School of Medicine, Kyoto University, Yoshida-Konoe-cho, Sakyo-ku, Kyoto 606-8501, Japan*
[3] *Division of Analytical and Physical Chemistry, Department of Analytical and Bioinorganic Chemistry, Kyoto Pharmaceutical University, Kyoto, 607-8414, Japan*
[4] *Division of Gastroenterology and Hematology/Oncology, Department of Medicine, Asahikawa Medical University, Asahikawa 078-8510, Japan*
[5] *Department of Gastrointestinal Immunology and Regenerative Medicine, Asahikawa Medical University, Asahikawa 078-8510, Japan*
[6] *Research Center for Environmental Risk, National Institute for Environmental Studies, 16-2 Onogawa, Tsukuba 305-8506, Japan*
[7] *Work Environment Research Group, National Institute of Occupational Health and Safety, 6-21-1 Nagao, Tama-ku, Kawasaki 214-8585, Japan*
[8] *National Science Laboratory, Faculty of Economics, Toyo University, 5-28-20, Hakusan, Bunkyo-ku, Tokyo 112-8606, Japan*
[9] *Department of Tumor Biology, Nagoya University Graduate School of Medicine, 65 Tsurumai-cho, Showa-ku, Nagoya 466-8550, Japan*

**Correspondence to: Professor Shinya Toyokuni, Department of Pathology and Biological Responses, Nagoya University Graduate School of Medicine, 65 Tsurumai-cho, Showa-ku, Nagoya, Japan. e-mail: toyokuni@med.nagoya-u.ac.jp*

Abstract

Exposure to asbestos is a risk for malignant mesothelioma (MM) in humans. Among the commercially used types of asbestos (chrysotile, crocidolite, and amosite), the carcinogenicity of chrysotile is not fully appreciated. Here, we show that all three asbestos types similarly induced MM in the rat peritoneal cavity and that chrysotile caused the earliest mesothelioma development with a high fraction of sarcomatoid histology. The pathogenesis of chrysotile-induced mesothelial carcinogenesis was closely associated with iron overload: repeated administration of an iron chelator, nitrilotriacetic acid, which promotes the Fenton reaction, significantly reduced the period required for carcinogenesis; massive iron deposition was found in the peritoneal organs with high serum ferritin; and homozygous deletion of the *CDKN2A/2B/ARF* tumour suppressor genes, the most frequent genomic alteration in human MM and in iron-induced rodent carcinogenesis, was observed in 92.6% of the cases studied with array-based comparative genomic hybridization. The induced rat MM cells revealed high expression of mesoderm-specific transcription factors, *Dlx5* and *Hand1*, and showed an iron regulatory profile of active iron uptake and utilization. These data indicate that chrysotile is a strong carcinogen when exposed to mesothelia, acting through the induction of local iron overload. Therefore, an intervention to remove local excess iron might be a strategy to prevent MM after asbestos exposure.

Keywords: asbestos; malignant mesothelioma; iron; array-based comparative genomic hybridization; *CDKN2A/2B*; *ARF*

Received 3 April 2012; Revised 28 June 2012; Accepted 11 July 2012

No conflicts of interest were declared.

Introduction

Natural fibrous minerals have been unexpected human carcinogens. Asbestos was valued as a miraculous stone because of heat-, acid-, and friction-resistance with economical merits, and thus was used from the ancient Egyptian era until the present century for wide industrial applications. However, in the 1960s, epidemiologists noticed the association between asbestos and malignant mesothelioma (MM) [1], which is a highly aggressive tumour when diagnosed, resistant to the currently available therapeutic modalities [2,3]. Due to a long incubation period, the expected peak year of MM in Japan is 2025, and over 100 000 people will suffer from MM in the coming 40 years [4]. This prompted us to elucidate the carcinogenic mechanism of asbestos-induced MM to discover clues for MM prevention. Lung cancer is also associated with asbestos exposure, but the situation is more complex because asbestos holds a synergistic effect with the carcinogenicity of tobacco [5].

In 1987, the International Agency for Research on Cancer defined all types of asbestos as a definite carcinogen to humans [1], but the appreciation of this declaration is quite different among countries [6]. Three kinds of asbestos fibres, chrysotile (white

asbestos), crocidolite (blue asbestos), and amosite (brown asbestos), have been used commercially, but the asbestos most frequently used has unequivocally been chrysotile [7]. Most Asian countries including China and India, and Russia, have not legally banned any type of asbestos. In Japan, the use of any type of asbestos was banned in September 2006 after the 'Kubota shock' in June 2005 [8]. Canada still maintains chrysotile mine operations [9].

Thus far, the notion that crocidolite and amosite, with their high iron contents (28.5% and 27.3%, respectively) [10], are far more carcinogenic than chrysotile (0.7%) has predominated [1]. However, controversies still exist [7]. In the present study, we used rat intraperitoneal experiments to evaluate the difference among the three asbestos types regarding carcinogenicity and the induced genomic alterations in MMs. The use of the peritoneal cavity is justified in that the interaction of asbestos and mesothelial cells is direct and maximal, presumably requiring less time for carcinogenesis [1], although respiratory factors have to be considered separately. Reportedly, inhalation of asbestos induces MM in a small percentage of animals [7], whereas intrapleural injection of asbestos takes a long time (mean survival ~2 years) for MM to develop, albeit with a high rate (25–69%) [1,11]. Here, we report that the progression of the disease (lethal MM) induced by chrysotile was the fastest, with similar genomic alterations shared by the three commercially used asbestos types.

Materials and methods

Measurements of asbestos fibres

Asbestos fibres were suspended and diluted in H_2O containing 1% NP40S (Tergitol; Sigma Aldrich, St Louis, MO, USA), followed by sonication for 30 min. We used a haemocytometer and microscopy to count the number and to measure the length of asbestos fibres for estimation by the use of Nikon ACT-1 software.

Carcinogenesis study using an animal model

The Animal Experiment Committee of the Graduate School of Medicine, Kyoto University and the Nagoya University Graduate School of Medicine approved these experiments. A suspension of UICC standard asbestos (chrysotile A, crocidolite, and amosite) in saline was prepared as described previously [12]. F_1 hybrid rats produced by crossing over between female Fischer 344 and male Brown-Norway rats (Charles River Japan, Yokohama, Japan) were used under specific pathogen-free conditions. A total of 141 F_1 rats were divided into the following five groups: untreated control ($N = 38$); chrysotile-treated ($N = 28$); crocidolite-treated ($N = 41$); amosite-treated ($N = 28$); and tangled multi-walled carbon nanotube (CNT; $N = 6$; Showa Denko, diameter $\phi = \sim 15$ nm). The characteristics of this nanotube are described elsewhere [13]. A total of 10 mg asbestos/CNT per rat was injected intraperitoneally with three injections (Figure 2a) when the F_1 rats reached 6 weeks of age (Supplementary Table 1). Some of the asbestos-treated rats were then given 80 mg/kg nitrilotriacetate (NTA) to enhance iron-catalysed Fenton reaction through separate intraperitoneal injections once a week for 16 weeks as described previously [14,15]. The animals were kept under close observation. When animals displayed massive ascites or distress, they were sacrificed. Control groups of rats, untreated or exposed to CNT, were sacrificed on day 940 and 742, respectively (Figure 2c). The rats were dissected and tissue samples were either fixed in phosphate-buffered 10% formalin for subsequent histological and immunohistochemical analyses, or snap-frozen in liquid nitrogen and stored at −80 °C until use. For a sub-acute study, the rats were subjected to a single intraperitoneal injection of 5 mg of chrysotile ($N = 6$), crocidolite ($N = 6$), and amosite ($N = 6$), respectively. Control rats ($N = 3$) were injected with saline. After 2 weeks, half of the asbestos-treated rats were injected intraperitoneally with NTA (80 mg/kg) and sacrificed 24 h afterwards. Rats injected with NTA without prior exposure to asbestos were also included as a control ($N = 3$).

Collection of normal control mesothelial cells from rats

Age-matched male rats were dissected and control mesothelial cells were collected as previously described [16].

Materials

All of the chemicals used were of analytical quality.

Array-based comparative genomic hybridization (aCGH)

We performed aCGH using Rat Genome CGH Microarray 244A (G4435A; Agilent Technologies, Santa Clara, CA, USA) according to the manufacturer's protocol. DNA from MM samples was labelled with Cy-5, while DNA from normal kidney, which was used as a reference, was labelled with Cy-3 for each array. The data obtained were analysed with Genomic Workbench Standard Edition 5.0 (Agilent Technologies). Prior to hierarchical clustering based on the aCGH profiles, statistically significant regions of copy number aberration were determined by the ADM-2 algorithm according to the sensitivity threshold at 10.0. The clustering procedure was conducted using the Pearson correlation similarity measure and complete linkage algorithm. We statistically evaluated the magnitude of chromosomal aberrations in the genome of each tumour as follows: an average of squares of $\log_2$ ratios between two-colour

hybridization signals for all the probes on the microarray was compared among each group by using the unpaired t-test.

Array-based CGH data may be found under the following GEO accession: GSE36577.

Genome copy analysis

Genomic DNA was extracted by using the DNeasy Blood and Tissue Kit (QIAGEN GmbH, Hilden, Germany). Quantitative PCR analysis was performed using the Platinum SYBR Green qPCR SuperMix UDG Kit (Invitrogen, Carlsbad, CA, USA) and Real-time PCR System 7300 (Applied Biosystems, Foster City, CA, USA). Primer sequences are described in Supplementary Table 2.

Fluorescence *in situ* hybridization (FISH)

Bacterial artificial chromosome clones (CH230-163D24) were purchased from http://bacpac.chori.org/ for *CDKN2A/2B*. Fluorescent probes were labelled by incorporating Green-dUTP (Vysis; Abbott Laboratories, Abbott Park, IL, USA) into newly synthesized DNA via the Nick Translation Kit (Vysis). Fluorescence *in situ* hybridization was performed using the probes, the Paraffin Pretreatment Kit, and LSI/WCP Hybridization Buffer (Vysis) according to the manufacturer's protocol. Briefly, paraffin sections were treated with protease, and after denaturation, the probes were hybridized to nuclear DNA, counterstained with DAPI, and visualized using a fluorescence microscope.

Reverse transcription and real-time PCR

Total RNA was isolated from tissue samples using the RNeasy Mini Kit (QIAGEN). The isolated total RNA was then treated with DNase I (Invitrogen Life Technologies) to digest remnant genomic DNA. cDNA was synthesized from 4 μg of total RNA using the First-Strand cDNA Synthesis Kit (GE Healthcare Offices, Little Chalfont, Buckinghamshire, UK) with random primers. For real-time quantitative PCR analysis, the Platinum SYBR Green qPCR SuperMix UDG Kit (Invitrogen) and Real-time PCR System 7300 (Applied Biosystems) were used. Each target gene was assayed in triplicate. Primer sequences are described in Supplementary Table 2.

Antibodies

Anti-podoplanin rabbit polyclonal antibody (KS-17) was from Sigma. Anti-multi-cytokeratin mouse monoclonal antibody (RTU-AE1/AE3) was from Novocastra (Newcastle, UK). Anti-desmin mouse monoclonal antibody (clone D33) was from DAKO (Carpinteria, CA, USA). Anti-calretinin rabbit monoclonal antibody (clone SP13) was from Abcam (Cambridge, MA, USA). Anti-S-100 polyclonal antibody (clone D33) was from DAKO. Anti-C-ERC/mesothelin monoclonal antibody was from IBL (Takasaki, Gunma, Japan). Anti-8-hydroxy-2′-deoxyguanosine (8-OHdG) mouse monoclonal antibody N45.1 [17] and anti-rat DMT1 rabbit polyclonal antibody [18] were used.

Western blot analysis

Protein lysates were prepared by homogenizing the tissue samples in RIPA lysis buffer containing 0.2 mmol/l sodium orthovanadate (Na_3VO_4), 50 mmol/l sodium fluoride (NaF), 1 mmol/l dithiothreitol, and 5.7 mg/ml aprotinin. Western blot was performed as described previously [19].

Tissue array, histology, and immunohistochemical analysis

We randomly selected 21 cases of epithelioid mesothelioma (EM; seven cases each from the chrysotile, crocidolite, and amosite groups) and 21 cases of sarcomatoid mesothelioma (SM; seven cases each from the chrysotile, crocidolite, and amosite groups) for tissue array preparation, and included liver, spleen, and kidney specimens in each tissue array. Representative areas from tissue specimens were chosen and cores of 3 mm diameter were punched out from the paraffin blocks with a precision instrument (Tissue Microprocessor; Azumaya, Tokyo, Japan). Cores of 24 (6×4 array) in a group were embedded in a paraffin block. Tissue sections of 3 μm thickness were then subjected to either haematoxylin and eosin staining or Perl's iron staining. For immunohistochemical analysis, the avidin–biotin complex method with peroxidase was used as described previously [17]. Immunostaining results were mostly uniform in distribution and were thus evaluated by two registered pathologists (YO and ST) as positive (+), weakly positive (weak +) or negative.

Serum ferritin and N-ERC/mesothelin assay

Commercial kits were used to measure rat serum ferritin (Mitsubishi Chemical Safety Institute Ltd, Uto, Kumamoto, Japan) and mesothelin (Immuno-Biological Laboratories Co, Ltd, Takasaki, Gunma, Japan) [20].

Measurement of iron content

Iron concentration was determined by inductively coupled plasma-mass spectrometry using a Shimadzu ICPM-8500 (Shimadzu, Kyoto, Japan) as described previously [13].

Measurement of non-transferrin-bound iron (NTBI)

Serum NTBI concentrations were measured as described previously [21].

Statistical analysis

Kaplan–Meier and other statistical analyses were performed using SPSS software. p values for Kaplan–Meier analysis were calculated by the log-rank test. Other analyses used were the unpaired t-test, modified

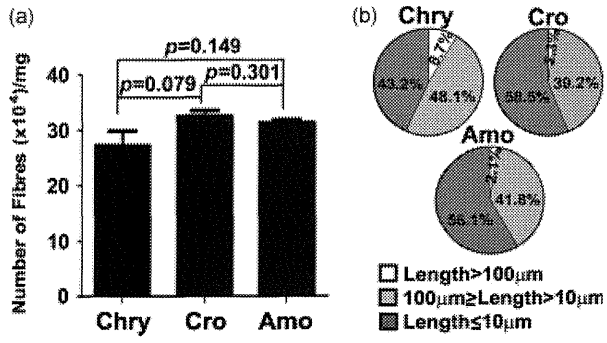

Figure 1. Characteristics of UICC asbestos fibres. (a) Number of fibres per weight (means ± SEM; $N = 15$). (b) Fraction of long and short fibres. Chry = chrysotile; Cro = crocidolite; Amo = amosite.

for unequal variances when necessary; Fisher's exact test; and the chi-square test. $p < 0.05$ was considered statistically significant.

Results

Re-evaluation of UICC-grade asbestos fibres

Three kinds of standard asbestos fibres obtained from Unio Internationalis Contra Cancrum (UICC) were re-evaluated. The number of fibres per weight was not significantly different among the three groups of asbestos fibres (Figure 1a). Chrysotile contained a higher fraction of longer fibres than those of the other two asbestos types (Figure 1b).

Comparison of mesothelial carcinogenesis by three different asbestos fibres and its modification by an iron chelator, NTA

We injected chrysotile, crocidolite or amosite fibres (10 mg; UICC) into the peritoneal cavity of F_1 hybrid rats from crosses of the Fischer-344 and Brown-Norway strains (Figure 2a). MM developed and infiltrated diffusely, concomitant with massive bloody ascites (Figure 2b) in 96.9% (94/97) of the rats injected with asbestos within 800 days after injection (Supplementary Table 1). Progression of the disease was fatal, due to malnutrition and organ failure via invasion (Figure 3a). We did not observe MM in two (2/41) rats of the crocidolite group and one (1/28) rat of the amosite group, which was confirmed histologically after sacrifice at day 812. Here, tangled CNTs, found to be non-carcinogenic [13], were included as a negative control of foreign fibrous material (Figure 2c). NTA alone does not induce MM, as described by us [14] and other investigators [22,23].

There are three distinct histological subtypes of MM: EM; SM; and biphasic mesothelioma (BM; a hybrid of EM and SM; Figures 2d and 3a). To confirm the mesothelial lineage of the tumours, we performed immunohistochemical analyses [Figure 3b, upper panel; positive for cytokeratin, calretinin, podoplanin (D2-40), and mesothelin; negative or weakly positive for desmin and S100]. SM revealed weaker cytokeratin, no calretinin, and no podoplanin, but intense mesothelin immunostaining. The immunohistochemistry results in tissue array samples are summarized in the lower panel of Figure 3b. Results of western blot analysis (podoplanin and calretinin) were positive for both types, albeit low positivity in SM (Figure 3c). Serum mesothelin at day 420/480 was significantly higher in the rats injected with asbestos than in control rats (Figure 3d).

We found that chrysotile fibres of the same weight caused a significantly shorter survival of rats via MM induction in comparison to crocidolite and amosite fibres (Figure 2c). Furthermore, we observed a higher frequency of SM in the chrysotile group, despite lack ($p = 0.111$ versus amosite) of statistical significance (Figure 2d). SM showed a significantly poorer prognosis than EM (Supplementary Figure 1). These results suggest that chrysotile fibres induce more aggressive disease than the other two fibres.

Chronic iron overload has been associated with carcinogenesis [24,25]. To evaluate the role of iron in asbestos-induced mesothelial carcinogenesis, we administered NTA, an iron chelator, to promote the Fenton reaction [26], to ~50% of the animals of each group (Supplementary Table 1). Unexpectedly, repeated weekly administration of NTA significantly accelerated mesothelioma development, not only in the crocidolite and amosite groups but also in the chrysotile group (Figure 2e). Males showed a faster progression of disease when treated with chrysotile fibres (Figure 2f), suggesting the influence of sex hormones either on the iron metabolism or on anti-oxidative mechanisms, as in the case with ferric NTA [27].

NTA promotes oxidative DNA modification in a sub-acute study

The ability of NTA to potentiate oxidative stress caused by asbestos fibres was tested in a sub-acute study of 3 weeks. Animals received intraperitoneal injection of 5 mg of chrysotile or crocidolite. Two weeks later, half of the animals received 80 mg/kg NTA and were killed after 24 h. Immunohistochemical analysis of 8-OHdG revealed that nuclear staining of mesothelia after asbestos and NTA is much stronger, with stromal oedema, than that of asbestos and a vehicle saline (Figure 4).

Association of local iron overload in asbestos-induced mesothelial carcinogenesis

To confirm the iron involvement in asbestos-induced mesothelioma, we performed Perl's iron staining of each of the abdominal organs collected from rats with MM in each asbestos group. The staining revealed prominent iron deposits in the spleen, liver, and kidney including surface mesothelial cells of rats injected with asbestos, whereas iron deposits were minimal in the age-matched controls (Figure 5a). Additional NTA treatment groups showed higher iron accumulation than

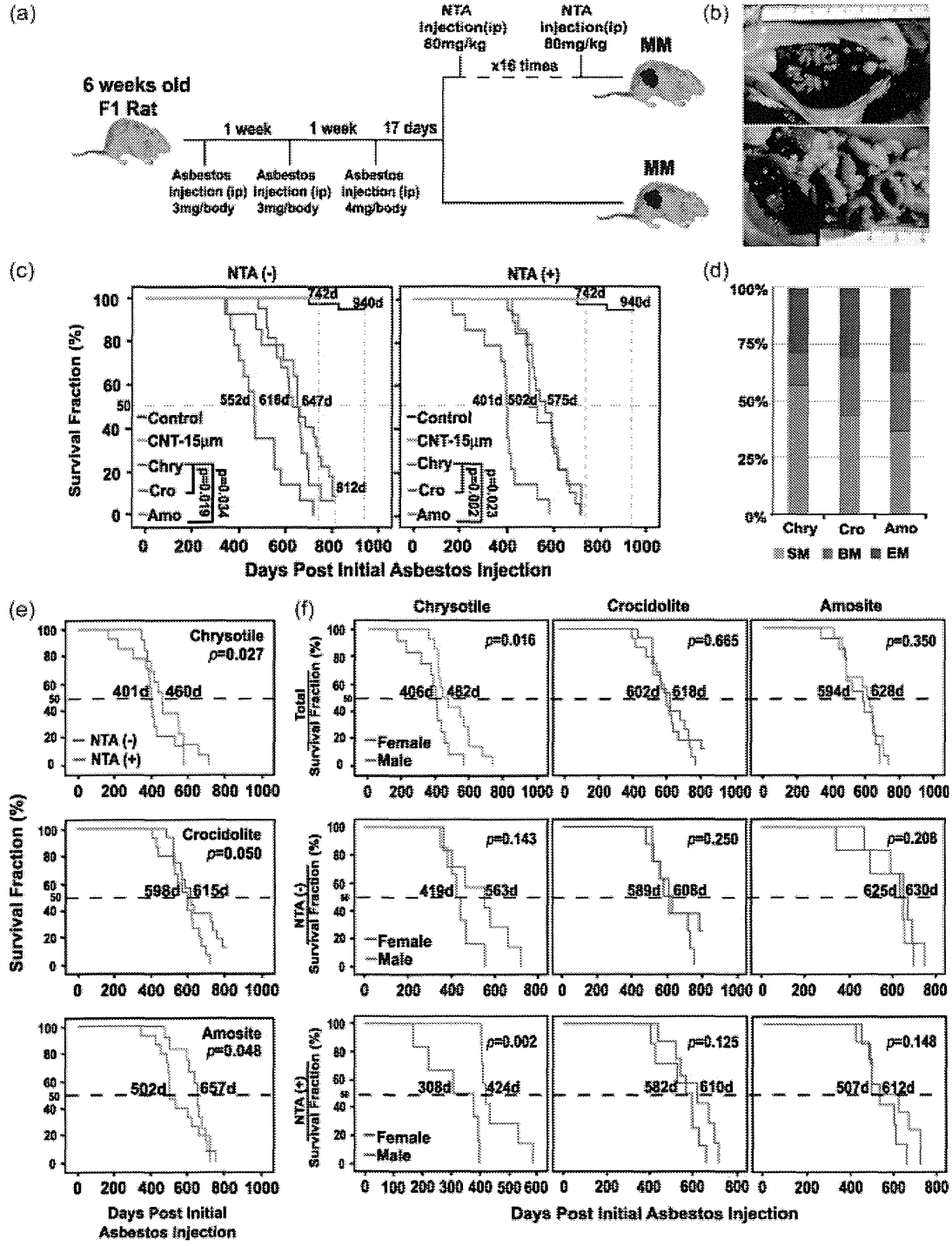

Figure 2. Induction of lethal peritoneal mesothelioma by three commercially used types of asbestos. (a) Carcinogenesis protocol. NTA = nitrilotriacetic acid, a synthetic iron chelator to promote the Fenton reaction; ip = intraperitoneal; MM = malignant mesothelioma. (b) Typical case of MM. Bloody ascites (upper panel) and multiple whitish tumours all over the peritoneum (lower panel). (c) Survival fraction regarding asbestos type. All the deaths were due to MM, except those in the untreated control group (see Supplementary Table 1 for details). Nanotube = tangled multi-walled carbon nanotube (diameter ϕ = 15 nm); d = days. p values for Kaplan–Meier analysis were calculated by the log-rank test. See text for details. (d) Ratios of histological type (EM = epithelioid mesothelioma; BM = biphasic mesothelioma; SM = sarcomatoid mesothelioma). (e) Survival fraction regarding asbestos type and NTA administration. (f) Survival fraction regarding asbestos type, sex, and NTA administration. See the Materials and methods and Results sections for details.

groups of asbestos alone. No iron accumulation near mesothelial cells was observed with tangled multi-walled CNTs that do not induce carcinogenesis. A detailed comparison of a variety of CNTs has been published elsewhere [13]. Iron measurements of the spleen and liver corroborated the results of Perl's iron staining, revealing significantly higher levels in all the asbestos groups than in the controls, which were further increased with additional NTA (Figure 5b). Serum from the 11 chrysotile-treated, 11 crocidolite-treated, and 15 amosite-treated rats 420 days after asbestos injection showed significantly higher levels of serum

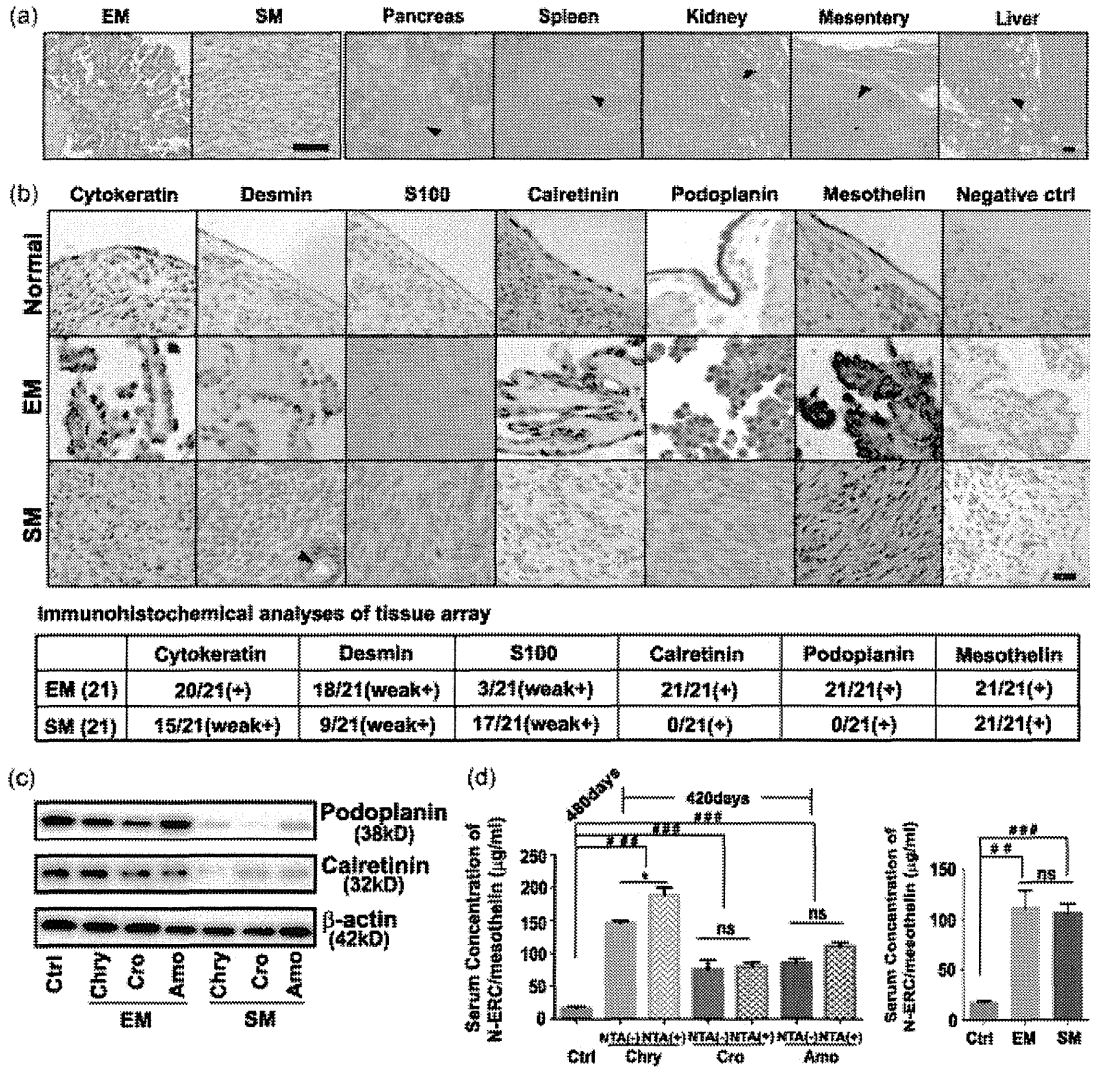

	Cytokeratin	Desmin	S100	Calretinin	Podoplanin	Mesothelin
EM (21)	20/21(+)	18/21(weak+)	3/21(weak+)	21/21(+)	21/21(+)	21/21(+)
SM (21)	15/21(weak+)	9/21(weak+)	17/21(weak+)	0/21(+)	0/21(+)	21/21(+)

Figure 3. Characteristics of asbestos-induced peritoneal mesothelioma in rats. (a) Histology of malignant mesothelioma. Invasion (arrowheads) is prominent in various organs (EM = epithelioid mesothelioma; SM = sarcomatoid mesothelioma; bar = 100 μm). (b) Immunohistochemical analysis for the evaluation of mesothelial origin (bar = 50 μm). The brown colour is the positivity except podoplanin (pink). Normal, rat control surface mesothelial cells; negative controls (ctrl) are shown as procedures without primary antibody (arrowhead, smooth muscle in a vessel). The inset table summarizes the immunohistochemical results. (c) Western blot analysis of the tumours. (d) Serum mesothelin (N-ERC; antigen at N-terminal portion) before apparent recognition of tumours (means ± SEM; $^{\#\#}p < 0.01$, $^{\#\#\#}p < 0.001$ versus untreated control; $^{*}p < 0.05$ between NTA(+) and NTA(−) in the same fibre group; ns = not significant). See the Materials and methods and Results sections for details.

ferritin than the controls, which was further increased with additional NTA (Figure 5c, left panel). We also measured the serum levels of NTBI, which revealed that the serum levels of NTBI were substantially reduced in the rats of the asbestos groups compared with the controls (Figure 5c, right panel), suggesting that a mechanism worked to withdraw 'catalytic' iron from serum.

Characteristics of iron metabolic pathways in asbestos-induced MM

We further examined the expression levels of genes associated with iron metabolism in MM. *DMT1* (*SLC11A2*) and *transferrin receptor 1* (*Tfrc*) are the genes involved in the uptake of iron from the extracellular compartment into the cells and its utilization, whereas *ferroportin 1* (*SLC40A1*) is involved in its export out of cells [28]. We found that the expression of *DMT1* and *Tfrc* was up-regulated in the MM tissues, whereas expression of *ferroportin 1* (Figure 5d) and *Dcytb* (duodenal cytochrome b; Supplementary Figure 3a) was down-regulated. Increased expression of *DMT1* in the mesothelioma samples was further confirmed by immunohistochemical staining (Supplementary Figure 2).

Evaluation of mesoderm-specific transcription factors

Two mesoderm-specific transcription factors (*Dlx5* and *Hand1*) were activated (Figure 5e). Among the expression levels of ectoderm- and endoderm-specific transcription factors, *Isl1*, *Pax6*, and *Mels1* were also increased in the mesothelioma samples; however, the increase was not prominent (Supplementary Figure 3).

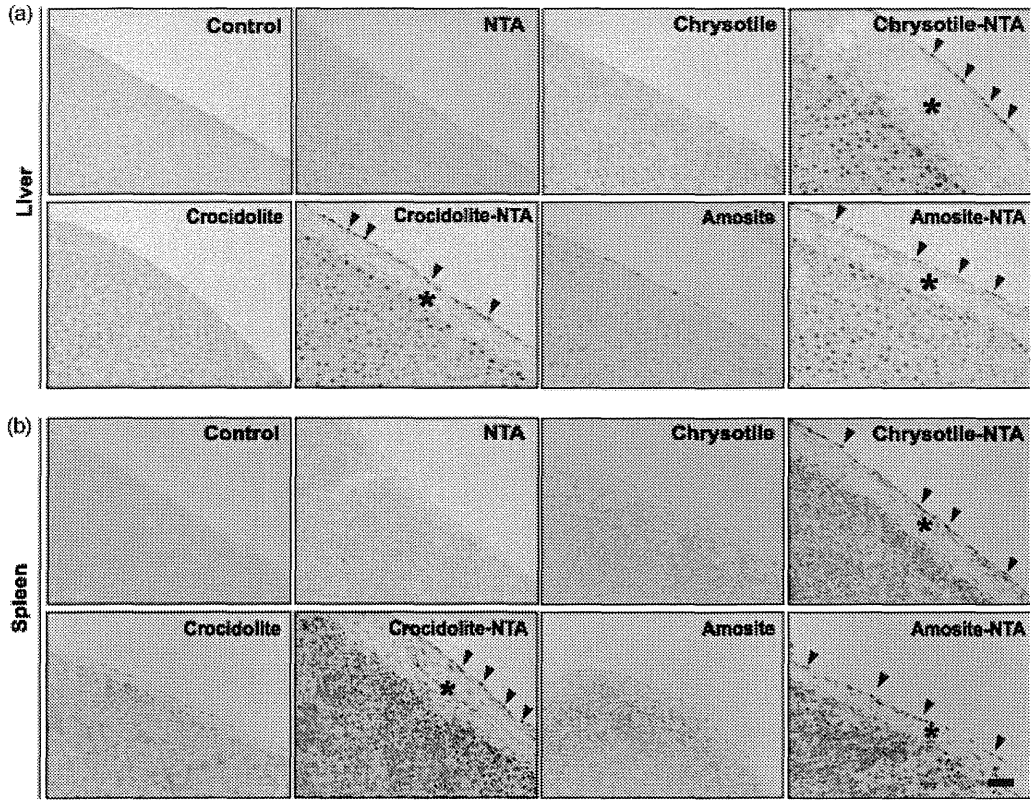

Figure 4. Immunohistochemical analysis of an oxidized DNA base, 8-hydroxy-2′-deoxyguanosine (8-OHdG) after treatment of asbestos followed by NTA. NTA (80 mg/kg) was administered intraperitoneally 2 weeks after ip administration of each asbestos fibre (5 mg). Note the nuclear positivity of mesothelial cells on the surface of (a) the liver and (b) the spleen. Representative figures are shown (bar = 50 μm). NTA enhanced the nuclear 8-OHdG positivity of the mesothelial cells, following different asbestos exposures (arrows, intensely stained nuclei of mesothelial cells; asterisk, oedema).

Genomic alterations in asbestos-induced MM

We then investigated the chromosomal aberrations in rat asbestos-induced MMs using the aCGH method (GEO accession: GSE36577). The results showed substantial genomic alterations over the whole genome, with many gains and losses of large chromosomal fragments (Figure 6a and Supplementary Figures 4a, 4b, and 5a). Many of the genomic alterations were not in common for each MM. However, high-copy amplification over a wide region of chromosomes 7 and 12 was observed in common, and deletion of genes across a wide region of the chromosome was observed in chromosomes 5 and 8 (Supplementary Figures 4a–4d). Chromosomal deletions in chromosomes 5 and 8 occurred more frequently in chrysotile-induced MMs (Supplementary Figure 4c), but encompassed narrower chromosomal regions globally in the genome in the chrysotile-induced MMs (Figure 6b). We found a common chromosomal deletion mapped to the chromosome 5q32 locus, containing the genes encoding the tumour suppressor genes *CDKN2A/2B/ARF*. Homozygous deletion of *CDKN2A/2B/ARF* was observed in the majority (92.6%; 25/27) of the rat MM samples, independent of the type of asbestos fibres used (Figure 6c). Loss of the *CDKN2A/2B/ARF* gene was confirmed by fluorescence *in situ* hybridization and quantitative real-time PCR analyses (Figures 6d and 6e). Furthermore, although we did not observe any change in the gene copy number of the two tumour suppressors *p53* and *NF2*, we found significant down-regulation in the expression levels of these two genes in the majority of the rat mesothelioma samples (Figure 6f). Such findings indicate that in addition to CDKN2A/2B/ARF and p53, loss of NF2 is also closely associated with MM development, although the loss of the NF2 pathway is likely to occur via epigenetic mechanisms. The three asbestos types were not differentiated with hierarchical clustering of the aCGH results.

Copy number changes associated with different histologies

As noted above, histologically, MMs can be classified into three distinct forms. We compared the aCGH results of these three different subtypes and found that SM showed the highest degree of genomic instability ($p < 0.05$) compared with the other subtypes (Supplementary Figures 5a and 5b). We also noticed that BM shows a frequent gain of gene copy number in chromosome 8, mapping to the region containing oncogenes such as *Birc2, Birc3*, and *YAP1* [29] (Supplementary Figure 5c). In addition, SM also had a more frequent amplified region in chromosome 7, which includes genes such as *Cct2* [30] and *Lyz* [31] (Supplementary Figure 5d).

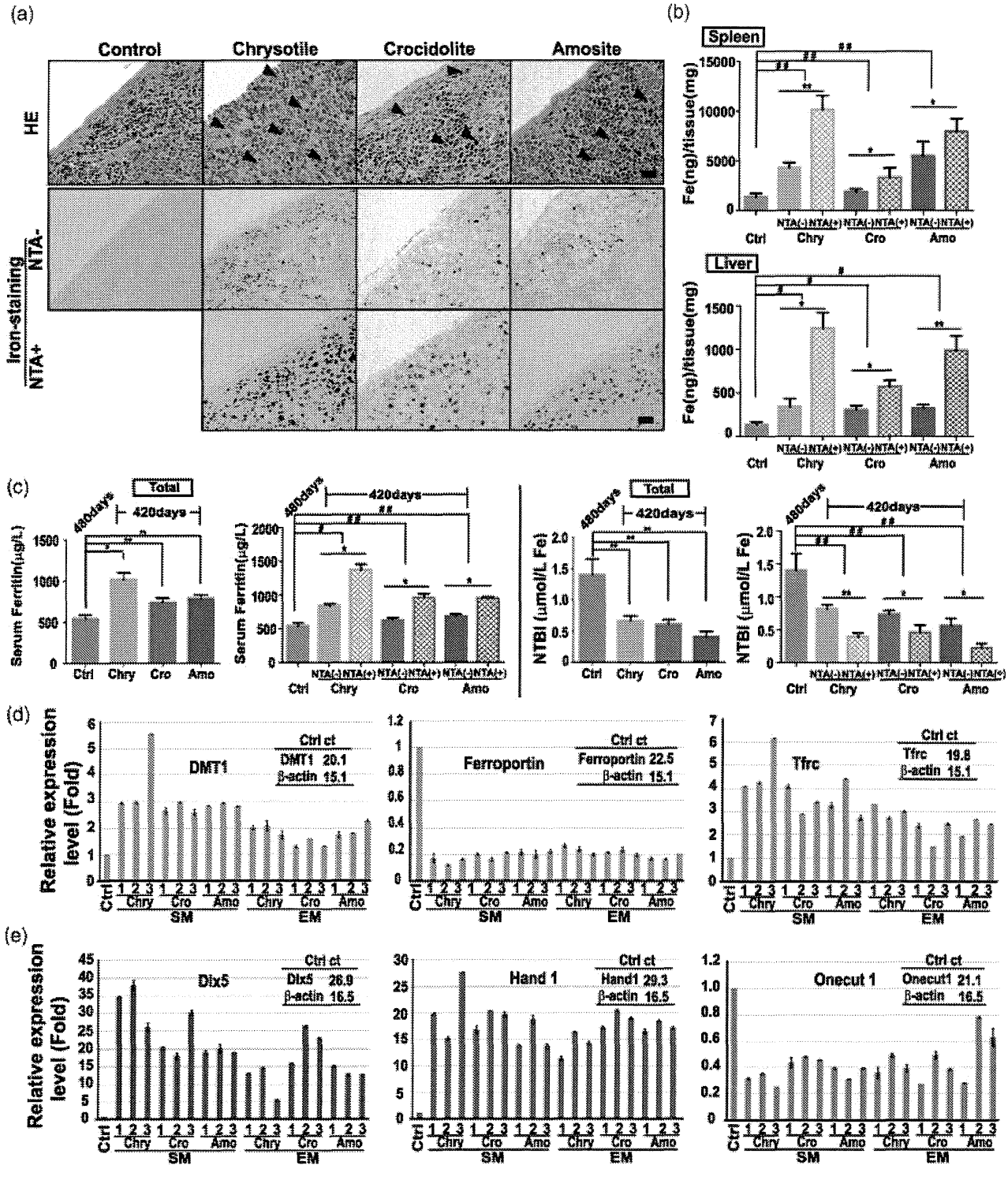

Figure 5. Iron overload in asbestos-induced mesothelial carcinogenesis and gene regulation in asbestos-induced mesothelioma. (a) Prominent deposition of iron in the spleen and mesothelial cells (upper row, haematoxylin and eosin staining; arrowheads, hemosiderin deposits; lower row, Perl's iron staining; bar = 100 μm; 50 μm in the insets). (b) Iron concentration in various organs of the peritoneal cavity regarding asbestos type and NTA administration (means ± SEM; $N = 5$ randomly selected among sacrificed animals after day 420). (c) Serum ferritin and NTBI (non-transferrin-bound iron) before apparent recognition of tumours (means ± SEM; $N = 5$–12). See Supplementary Table 1 for details. (d) Expression of iron-associated genes in the asbestos-induced mesothlioma. *DMT1, SLC11A2; ferroportin, SLC40A1; Tfrc, transferrin receptor 1* (CD71); Ctrl ct, control cycle times. Ctrl is the control mesothelial sample obtained by scraping rat solid organs as described in the Materials and methods section (means ± SD, triplicate). (e) Expression of mesoderm-specific transcription factors in the asbestos-induced mesothelioma. Sample numbers correspond to each other in d and e (means ± SD, triplicate).

J Pathol 2012; **228:** 366–377
www.thejournalofpathology.com

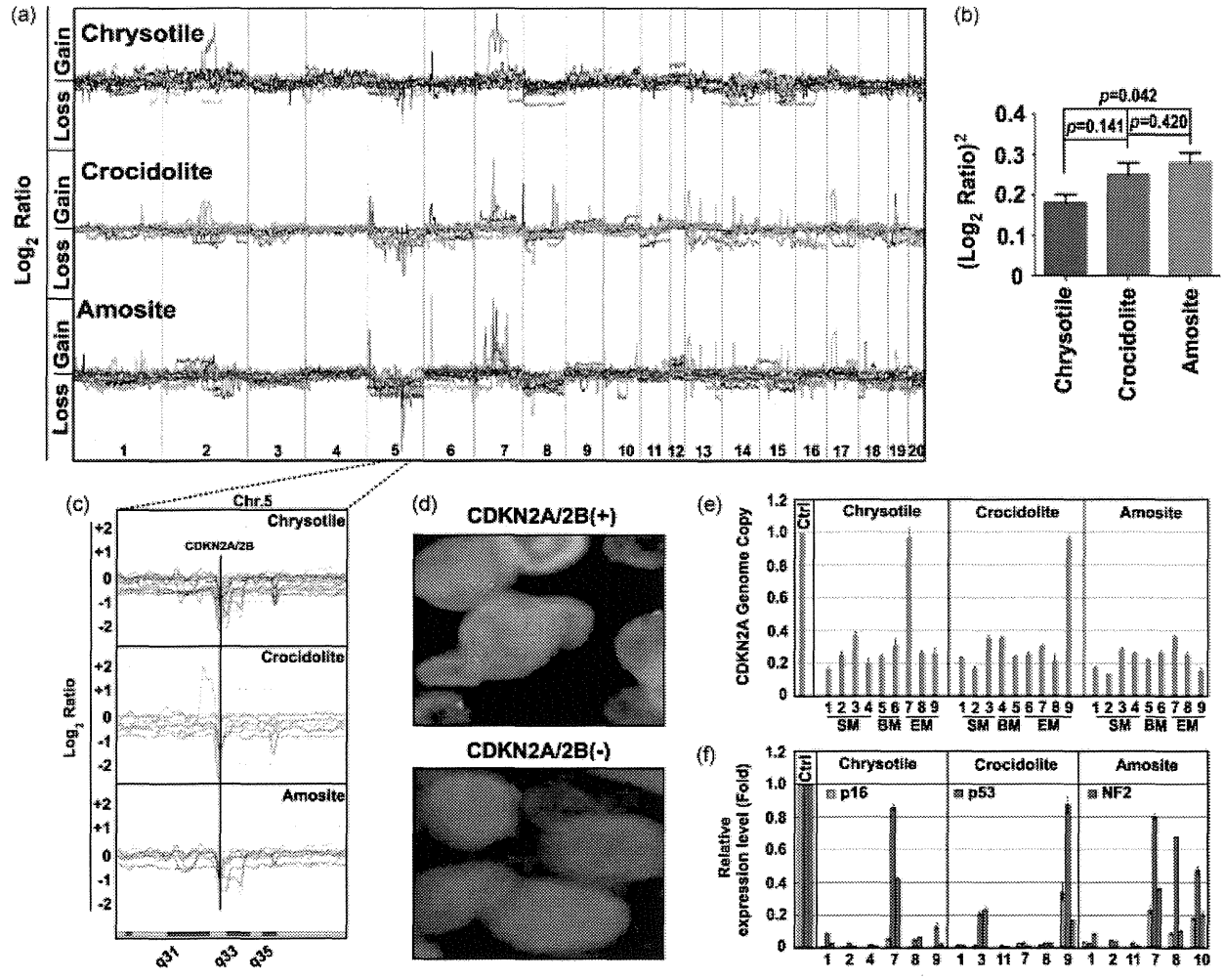

Figure 6. Massive genomic alteration with homozygous deletion of *CDKN2A/2B* is a hallmark of asbestos-induced mesothelioma. (a) Combined scheme of array-based comparative genome hybridization analysis ($N = 9$ for each asbestos, consisting of 3 EMs, 2–3 BMs, and 3–4 SMs, respectively). The three asbestos types were not differentiated with hierarchical clustering. (b) Quantitation of chromosomal aberration over the whole genome by ($\log_2$ ratio) [2]. Zero means no amplification/deletion (2N state), and the increased number indicates amplification/deletion with the same weight between 4N amplification and N (heterozygous) deletion (means ± SEM; SM, $N = 10$; BM, $N = 8$; EM, $N = 9$). (c) Homozygous deletion of *CDKN2A/2B* is observed in 25/27 cases (88.9% in chrysotile- or crocidolite-induced mesothelioma; 100% in amosite-induced mesothelioma). (d) Fluorescence *in situ* hybridization analysis to confirm the homozygous deletion of *CDKN2A/2B*. Pink dots are the signals under DAPI nuclear counter-staining. (e) Semi-quantitative PCR analysis for evaluation of the copy number of the *CDKN2A/2B* locus (means ± SD, triplicate). (f) Expression of *CDKN2A* (*p16*), *p53*, and *NF2*. Sample numbers correspond to each other in e and f (means ± SD, triplicate).

Discussion

Many animal experiments were performed regarding the carcinogenicity of asbestos in the 1970s and 1980s [1]. One of the fruitful outcomes was 'Stanton's hypothesis' on macrophage involvement that asbestos fibres longer than 8–20 μm and thinner than 0.25 μm more readily induce MMs [32,33]. The present experiments are a re-evaluation of those with modern molecular techniques under specific pathogen-free environments in the hope of understanding, preventing, and curing asbestos-induced mesothelial carcinogenesis. We also re-evaluated the UICC standard asbestos fibres reportedly produced in the 1990s and found that the fibre numbers per weight were not significantly different among the three commercial asbestos types, but that chrysotile contained a higher fraction of long fibres (Figure 1). We cannot rule out the possibility that a high fraction of longer fibres affected the carcinogenicity, but these are the standard types of asbestos used in the scientific community.

MMs induced in rats were similar to their human counterparts histologically as well as immunohistochemically [34], and from the standpoint of serum marker [35,36] (Figure 3). The data presented here point towards the idea that chrysotile is the fastest to induce MM among the commercial types of asbestos, with a higher fraction of a more malignant SM type (Figure 2 and Supplementary Figure 1). Although chrysotile itself contains a small amount of iron, iron overload appears to have played an important role in chrysotile-induced mesothelial carcinogenesis, as did crocidolite and amosite. Furthermore, the iron-overloaded condition was most prominent with chrysotile, as seen by iron staining, measurements, and serum ferritin levels (Figure 5). This is presumably via

its high haemolytic activity and the associated catalytic activity of iron, making the surface of asbestos a niche for oxidative modification [37], and is consistent with the cultured cell experiments using iron-loaded synthetic chrysotile [38]. Interestingly, the genomic aberration area was narrower than the other two types of asbestos (Figure 6b), suggesting that chrysotile attack is more pinpoint and is in the proximity of genomic DNA. This pathogenic mechanism of iron involvement was demonstrated further by the significant promotional effect of NTA (Figure 2f) and by the characteristic pattern of genomic alterations (Figure 6c) in the iron-induced rat tumours [39]. No iron accumulation, in our recent publication [13], near mesothelial cells with tangled CNT (no MM formation; Figure 2c) confirms the involvement of iron overload in mesothelial carcinogenesis.

NTA, a synthetic aminopolycarboxylic acid, binds with hydrogen bonding only three or four out of six ligands of ferric iron, thus leaving free catalytic ligands at neutral pH [40]. We showed that even a single intraperitoneal injection of NTA enhanced the *in vivo* oxidative DNA modification of mesothelial cells 2 weeks after asbestos administration (Figure 4). The significantly earlier occurrence of MM in male rats than in females only in the chrysotile group (Figure 2f) may result from the sex difference in iron metabolism and suggests a strong commitment of iron overload in chrysotile-induced carcinogenesis.

In animal models without genetic engineering, homozygous deletion of *CDKN2A/2B/ARF* is observed only in ferric-NTA-induced renal cell carcinoma of rats [41] and in sarcomatoid mesothelioma of rats induced by ferric saccharate with NTA [15,39], as far as we know. Therefore, we believe that this genetic alteration represents an 'iron overload' signature. The present data strongly support the role of iron overload in chrysotile-induced carcinogenesis. This aberration causes simultaneous loss of both the RB and the p53 (via ARF) tumour suppressive pathways [39]. Since this is a most frequently observed genomic alteration in human MMs [42], this rat model precisely mimics human MMs. Hierarchical clustering did not detect an asbestos-specific difference in the array CGH profiles, though we found a tendency of more frequent chromosomal deletions in chromosomes 5 and 8 but globally narrower chromosomal aberration in chrysotile-induced MMs (Figure 6 and Supplementary Figure 4). Inclusion of *Yap1* amplification (Supplementary Figure 5c) in the Hippo pathway [43] confirms that the present rat model is similar to the human counterparts. Recently, an aCGH analysis of murine MM (*NF2*$^{+/-}$ and wild-type) cell lines was reported although a low-density BAC CGH array was used. Alteration of *CDKN2A* and *CDKN2B* was observed at 56% and 60%, respectively [44]. Their study does not rule out the possibility of a deletional event during the establishment of cell lines as described previously [45].

We observed that there was a tendency for iron to accumulate in cells (macrophages, mesothelial cells, and other parenchymal cells) after exposure to each asbestos type, concomitant with low serum NTBI (Figure 5). This precisely mimics the inflammatory condition caused by bacterial infection, where the host undertakes to deprive bacteria of available iron [46]. Of note, an iron regulatory profile of this kind was also observed in the asbestos-induced MMs (Figure 5d).

Based on direct and indirect evidence, we propose that the iron overload condition is the key pathological condition during mesothelial carcinogenesis by all the commercially used asbestos types. Therefore, iron modulation via phlebotomy, iron chelators or any other means to remove local excess iron might be a hopeful strategy for preventing MM.

Interestingly, we found that asbestos-induced MMs are driven by the mesoderm-specific transcription factors DLX5 [47] and HAND1 [48], but not by ONE-CUT 1 (HNF6) [49] (Figure 4e). DLX5 expression was much stronger in the asbestos-induced MM than that induced by iron saccharate, but an ectoderm-associated transcription factor, PAX 6, was commonly overexpressed (Supplementary Figure 4c) [15].

The major limitation of our study is that intraperitoneal administration differs from the situation of human environmental exposure. We understand that present experiments evaluated the carcinogenicity of each fibre type on mesothelial cells at direct contact. Other objective methods to evaluate how easily each fibre reaches the pleural mesothelial cells via a respiratory pathway are mandatory and currently under development.

In conclusion, chrysotile is a strong carcinogen that acts through the induction of local iron overload *in vivo* when it reachs mesothelial cells. Therefore, more appropriate measures have to be taken to reduce environmental cancer risk in this era of human longevity. Since every type of commercially used asbestos causes local 'iron overload' pathology, iron modulation to remove local excess iron [40] might be an encouraging strategy to prevent MM in people who have already been exposed to asbestos. Following the current study, the effects of chrysotile on lung carcinogenesis also require immediate re-evaluation.

Acknowledgment

This study was supported by a MEXT grant (Special Coordination Funds for Promoting Science and Technology); the Princess Takamatsu Cancer Research Fund (10-24213); a Grant-in-Aid for Cancer Research from the Ministry of Health, Labor, and Welfare of Japan; a Grant-in-Aid from the Ministry of Education, Culture, Sports, Science and Technology of Japan; a grant of Long-range Research Initiative by the Japan Chemical Industry Association; and a grant from Takeda Science Foundation.

Abbreviations

aCGH	array-based comparative genomic hybridization
ANOVA	analysis of variance
BAC	bacterial artificial chromosome
BM	biphasic (malignant) mesothelioma
CNT	carbon nanotube
EM	epithelioid (malignant) mesothelioma
FISH	fluorescence *in situ* hybridization
MM	malignant mesothelioma
NTA	nitrilotriacetic acid (nitrilotriacetate)
NTBI	non-transferrin-bound iron
8-OHdG	8-hydroxy-2′-deoxyguanosine
PBS	phosphate-buffered saline
RPMC	rat peritoneal mesothelial cells
SM	sarcomatoid (malignant) mesothelioma
UICC	Unio Internationalis Contra Cancrum

Author contribution statement

LJ and ST conceived and designed the experiments. LJ, SA, HN, HO, SHC, YO, Y. Yoshikawa, KI, and KS performed the experiments. HY, YK, TT, and ST analysed the data. Y. Yamashita, SH, YS, and NK contributed materials. LJ and ST wrote the paper.

References

1. IARC, World Health Organization. Asbestos (chrysotile, amosite, crocidolite, tremolite, actinolite, and anthophyllite). *IARC Monographs on the Evaluation of Carcinogenic Risks to Humans. A Review of Human Carcinogens; Part C: Arsenic, Metals, Fibres, and Dusts*. IARC: Lyon, 2012; 219–309.
2. Roggli VL, Oury TD, Sporn TA (eds). *Pathology of Asbestos-Associated Diseases* (2nd edn). Springer Verlag: New York, 2004.
3. Robinson B, Musk A, Lake R. Malignant mesothelioma. *Lancet* 2005; **366**: 397–408.
4. Robinson B, Lake R. Advances in malignant mesothelioma. *N Engl J Med* 2005; **353**: 1591–1603.
5. Alberg AJ, Ford JG, Samet JM. Epidemiology of lung cancer: ACCP evidence-based clinical practice guidelines (2nd edition). *Chest* 2007; **132**: 29S–55S.
6. Editorials this week: asbestos scandal (16 December 2010). *Nature* 2010; **468**: 868.
7. Smith AH, Wright CC. Chrysotile asbestos is the main cause of pleural mesothelioma. *Am J Ind Med* 1996; **30**: 252–266.
8. 79 Kubota workers killed by asbestos over 26 years. *The Daily Yomiuri*. The Yomiuri Shimbun: Japan; 30 June 2005.
9. Greenberg M. The defence of chrysotile, 1912–2007. *Int J Occup Environ Health* 2008; **14**: 57–66.
10. Hardy JA, Aust AE. Iron in asbestos chemistry and carcinogenicity. *Chem Rev* 1995; **95**: 97–118.
11. Wagner JC, Berry G, Timbrell V. Mesotheliomata in rats after inoculation with asbestos and other materials. *Br J Cancer* 1973; **28**: 173–185.
12. Jiang L, Nagai H, Ohara H, *et al*. Characteristics and modifying factors of asbestos-induced oxidative DNA damage. *Cancer Sci* 2008; **99**: 2142–2151.
13. Nagai H, Okazaki Y, Chew SH, *et al*. Diameter of multi-walled carbon nanotubes is a critical factor in mesothelial injury and subsequent carcinogenesis. *Proc Natl Acad Sci U S A* 2011; **108**: E1330–E1338.
14. Okada S, Hamazaki S, Toyokuni S, *et al*. Induction of mesothelioma by intraperitoneal injections of ferric saccharate in male Wistar rats. *Br J Cancer* 1989; **60**: 708–711.
15. Hu Q, Akatsuka S, Yamashita Y, *et al*. Homozygous deletion of *CDKN2A/2B* is a hallmark of iron-induced high-grade rat mesothelioma. *Lab Invest* 2010; **90**: 360–373.
16. Jiang L, Yamashita Y, Toyokuni S. A novel method for efficient collection of normal mesothelial cells *in vivo*. *J Clin Biochem Nutr* 2010; **46**: 265–268.
17. Toyokuni S, Tanaka T, Hattori Y, *et al*. Quantitative immunohistochemical determination of 8-hydroxy-2′-deoxyguanosine by a monoclonal antibody N45.1: its application to ferric nitrilotriacetate-induced renal carcinogenesis model. *Lab Invest* 1997; **76**: 365–374.
18. Shirase T, Mori K, Okazaki Y, *et al*. Suppression of *SLC11A2* expression is essential to maintain duodenal integrity during dietary iron overload. *Am J Pathol* 2010; **177**: 677–685.
19. Toyokuni S, Kawaguchi W, Akatsuka S, *et al*. Intermittent microwave irradiation facilitates antigen–antibody reaction in western blot analysis. *Pathol Int* 2003; **53**: 259–261.
20. Hagiwara Y, Hamada Y, Kuwahara M, *et al*. Establishment of a novel specific ELISA system for rat N- and C-ERC/mesothelin. Rat ERC/mesothelin in the body fluids of mice bearing mesothelioma. *Cancer Sci* 2008; **99**: 666–670.
21. Sasaki K, Ikuta K, Tanaka H, *et al*. Improved quantification for non-transferrin-bound iron measurement using high-performance liquid chromatography by reducing iron contamination. *Mol Med Rep* 2011; **4**: 913–918.
22. Mottola HA. Nitrilotriacetic acid as a chelating agent: applications, toxicology, and bio-environmental impact. *Toxicol Environ Chem Rev* 1974; **71**: 99–161.
23. Anderson RL, Bishop WE, Campbell RL. A review of the environmental and mammalian toxicology of nitrilotriacetic acid. *Crit Rev Toxicol* 1985; **15**: 1–102.
24. Toyokuni S. Iron-induced carcinogenesis: the role of redox regulation. *Free Radic Biol Med* 1996; **20**: 553–566.
25. Toyokuni S. Role of iron in carcinogenesis: cancer as a ferrotoxic disease. *Cancer Sci* 2009; **100**: 9–16.
26. Toyokuni S, Sagripanti JL. Iron-mediated DNA damage: sensitive detection of DNA strand breakage catalyzed by iron. *J Inorg Biochem* 1992; **47**: 241–248.
27. Toyokuni S, Okada S, Hamazaki S, *et al*. Combined histochemical and biochemical analysis of sex hormone dependence of ferric nitrilotriacetate-induced renal lipid peroxidation in ddY mice. *Cancer Res* 1990; **50**: 5574–5580.
28. Dunn L, Rahmanto Y, Richardson D. Iron uptake and metabolism in the new millennium. *Trends Cell Biol* 2007; **17**: 93–100.
29. Cheng L, Zhou Z, Flesken-Nikitin A, *et al*. Rb inactivation accelerates neoplastic growth and substitutes for recurrent amplification of *cIAP1*, *cIAP2* and *Yap1* in sporadic mammary carcinoma associated with p53 deficiency. *Oncogene* 2010; **29**: 5700–5711.
30. Lin YF, Tsai WP, Liu HG, *et al*. Intracellular beta-tubulin/chaperonin containing TCP1-beta complex serves as a novel chemotherapeutic target against drug-resistant tumors. *Cancer Res* 2009; **69**: 6879–6888.
31. Lee HS, Park MH, Yang SJ, *et al*. Novel candidate targets of Wnt/beta-catenin signaling in hepatoma cells. *Life Sci* 2007; **80**: 690–698.
32. Stanton MF, Layard M, Tegeris A, *et al*. Relation of particle dimension to carcinogenicity in amphibole asbestoses and other fibrous minerals. *J Natl Cancer Inst* 1981; **67**: 965–975.

33. Donaldson K, Aitken R, Tran L, *et al*. Carbon nanotubes: a review of their properties in relation to pulmonary toxicology and workplace safety. *Toxicol Sci* 2006; **92**: 5–22.
34. Husain AN, Colby TV, Ordonez NG, *et al*. Guidelines for pathologic diagnosis of malignant mesothelioma: a consensus statement from the International Mesothelioma Interest Group. *Arch Pathol Lab Med* 2009; **133**: 1317–1331.
35. Shiomi K, Miyamoto H, Segawa T, *et al*. Novel ELISA system for detection of N-ERC/mesothelin in the sera of mesothelioma patients. *Cancer Sci* 2006; **97**: 928–932.
36. Hassan R, Remaley AT, Sampson ML, *et al*. Detection and quantitation of serum mesothelin, a tumor marker for patients with mesothelioma and ovarian cancer. *Clin Cancer Res* 2006; **12**: 447–453.
37. Nagai H, Ishihara T, Lee W-H, *et al*. Asbestos surface provides a niche for oxidative modification. *Cancer Sci* 2012; **102**: 2118–2125.
38. Gazzano E, Turci F, Foresti E, *et al*. Iron-loaded synthetic chrysotile: a new model solid for studying the role of iron in asbestos toxicity. *Chem Res Toxicol* 2007; **20**: 380–387.
39. Toyokuni S. Mysterious link between iron overload and *CDKN2A/2B*. *J Clin Biochem Nutr* 2011; **48**: 46–49.
40. Toyokuni S. Iron as a target of chemoprevention for longevity in humans. *Free Radic Res* 2011; **45**: 906–917.
41. Tanaka T, Iwasa Y, Kondo S, *et al*. High incidence of allelic loss on chromosome 5 and inactivation of $p15^{INK4B}$ and $p16^{INK4A}$ tumor suppressor genes in oxystress-induced renal cell carcinoma of rats. *Oncogene* 1999; **18**: 3793–3797.
42. Xio S, Li D, Vijg J, *et al*. Codeletion of *p15* and *p16* in primary malignant mesothelioma. *Oncogene* 1995; **11**: 511–515.
43. Sekido Y. Inactivation of Merlin in malignant mesothelioma cells and the Hippo signaling cascade dysregulation. *Pathol Int* 2011; **61**: 331–344.
44. Jean D, Thomas E, Manie E, *et al*. Syntenic relationships between genomic profiles of fiber-induced murine and human malignant mesothelioma. *Am J Pathol* 2011; **178**: 881–894.
45. Foster SA, Wong DJ, Barrett MT, *et al*. Inactivation of p16 in human mammary epithelial cells by CpG island methylation. *Mol Cell Biol* 1998; **18**: 1793–1801.
46. Miceli MH, Dong L, Grazziutti ML, *et al*. Iron overload is a major risk factor for severe infection after autologous stem cell transplantation: a study of 367 myeloma patients. *Bone Marrow Transpl* 2006; **37**: 857–864.
47. Miyama K, Yamada G, Yamamoto T, *et al*. A BMP-inducible gene, *dlx5*, regulates osteoblast differentiation and mesoderm induction. *Dev Biol* 1999; **208**: 123–133.
48. Firulli A, McFadden D, Lin Q, *et al*. Heart and extra-embryonic mesodermal defects in mouse embryos lacking the bHLH transcription factor Hand1. *Nature Genet* 1998; **18**: 266–270.
49. Khoo M, McQuade L, Smith M, *et al*. Growth and differentiation of embryoid bodies derived from human embryonic stem cells: effect of glucose and basic fibroblast growth factor. *Biol Reprod* 2005; **73**: 1147–1156.

SUPPORTING INFORMATION ON THE INTERNET

The following supporting information may be found in the online version of this article.

Figure S1. Survival fraction regarding asbestos type, histological type, and NTA administration.

Figure S2. Immunohistochemistry of DMT1.

Figure S3. Expression analysis of asbestos-induced rat MMs.

Figure S4. Analysis of array-based comparative genomic hybridization from the viewpoint of each chromosome and asbestos type.

Figure S5. Analysis of array-based comparative genomic hybridization from the viewpoint of histology.

Table S1. Incidence of asbestos-induced malignant mesothelioma.

Table S2. Primers used for quantitative real-time PCR analysis.

TGF-β synergizes with defects in the Hippo pathway to stimulate human malignant mesothelioma growth

Makiko Fujii,[1] Takeshi Toyoda,[5] Hayao Nakanishi,[2] Yasushi Yatabe,[3] Ayuko Sato,[6] Yasue Matsudaira,[1] Hidemi Ito,[1] Hideki Murakami,[1] Yutaka Kondo,[1] Eisaku Kondo,[2] Toyoaki Hida,[4] Tohru Tsujimura,[6] Hirotaka Osada,[1,7] and Yoshitaka Sekido[1,7]

[1]Division of Molecular Oncology and [2]Division of Oncological Pathology, Aichi Cancer Center Research Institute; and [3]Department of Pathology and Molecular Diagnostics and [4]Department of Thoracic Oncology, Aichi Cancer Center Hospital; Aichi Cancer Center, Chikusa-ku, Nagoya 464-8681, Japan
[5]Division of Pathology, National Institute of Health Sciences, Setagaya-ku, Tokyo 158-8501, Japan
[6]Department of Pathology, Hyogo College of Medicine, Nishinomiya, Hyogo 663-8501, Japan
[7]Department of Cancer Genetics, Program in Function Construction Medicine, Nagoya University Graduate School of Medicine, Showa-ku, Nagoya 466-8550, Japan

Malignant mesothelioma (MM) is an incurable malignancy that is caused by exposure to asbestos and is accompanied by severe fibrosis. Because MM is usually diagnosed at an advanced stage and clinical identification of early lesions is difficult, its molecular pathogenesis has not been completely elucidated. Nearly 75% of MM cases have inactivating mutations in the *NF2* (*neurofibromatosis type 2*; Merlin) gene or in downstream signaling molecules of the Hippo signaling cascade, which negatively regulates the transcription factor Yes-associated protein (YAP). In this study, we demonstrate a functional interaction between the Hippo and TGF-β pathways in regulating connective tissue growth factor (CTGF). Expression of CTGF in MM cells was induced by the formation of a YAP–TEAD4–Smad3–p300 complex on the *CTGF* promoter. Knocking down CTGF expression in MM cells prolonged the survival of xenografted mice, and a significant association was seen between CTGF expression and extracellular matrix deposition in MM xenografts and in patient tissue specimens. We further suggest that CTGF may influence the malignancy of mesothelioma because of the different histological expression patterns observed in human MM tissues. These data suggest that CTGF is an important modulator of MM growth and pathology and represents a novel therapeutic target for this disease.

CORRESPONDENCE
Makiko Fujii:
fujiim@aichi-cc.jp
OR
Yoshitaka Sekido:
ysekido@aichi-cc.jp

Abbreviation used: CC, coiled-coil; ChIP, chromatin immunoprecipitation; CTGF, connective tissue growth factor; ECM, extracellular matrix; MM, malignant mesothelioma; mRNA, messenger RNA; shRNA, short hairpin RNA; TEAD, TEA domain family member; YAP, Yes-associated protein.

Malignant mesothelioma (MM), arising from serosal cells of the pleural, peritoneal, and pericardial cavities, has a poor prognosis because it is frequently diagnosed at advanced stages. The primary cause of this disease has often been linked to asbestos exposure, and the number of patients worldwide is predicted to peak in the next two decades (Robinson and Lake, 2005; Murayama et al., 2006). The latent period between first exposure to asbestos and onset of the disease is ~20–40 yr, and the first symptom is insidious and may include chest pain and breathlessness. Although there has been significant recent progress in clinical treatment with combination chemotherapies, a curative therapy for MM is still unknown, with the median survival ranging between 9 and 17 mo from the first diagnosis (Tsao et al., 2009).

The involvement of tumor suppressor genes, including $p16^{INK4a}/p14^{ARF}$ and *NF2* (*neurofibromatosis type 2*), has been demonstrated to be crucial in the development of various MMs (Bianchi et al., 1995; Sekido et al., 1995). The *NF2* gene, known to be responsible for NF2 syndrome, encodes Merlin, and deletions or mutations of this gene were found in 40–50% of MMs. The downstream signaling of Merlin is the mammalian Hippo cascade, which was originally identified by genetic studies in *Drosophila melanogaster* (Hay and Guo, 2003; Ryoo and Steller, 2003; Wu et al., 2003;

The Rockefeller University Press $30.00
J. Exp. Med. Vol. 209 No. 3 479-494
www.jem.org/cgi/doi/10.1084/jem.20111653